NASA CONTRACTOR REPORT

NASA CR-1571

PRIMARY LOOP ELECTROMAGNETIC PUMP DESIGN

by J. W. Gahan, P. T. Pileggi, and A. H. Powell

Prepared by
GENERAL ELECTRIC CO.
Cincinnati, Ohio
for Lewis Research Center

NATIONAL AERONAUTICS AND SPACE ADMINISTRATION • WASHINGTON, D. C. • JUNE 1970

1. Report No. NASA CR-1571	2. Government Accession No.	3. Recipient's Catalog No.
4. Title and Subtitle PRIMARY LOOP ELECTROMAGNETIC PUMP DESIGN		5. Report Date June 1970 6. Performing Organization Code
7. Author(s) J. W. Gahan, P. T. Pileggi, and A. H. Powell		8. Performing Organization Report No. GESP-337
9. Performing Organization Name and Address General Electric Co. Missile and Space Division Cincinnati, Ohio 45215		10. Work Unit No. 11. Contract or Grant No. NAS 3-10604 13. Type of Report and Period Covered Contractor Report
12. Sponsoring Agency Name and Address National Aeronautics and Space Administration Washington, D.C. 20546		14. Sponsoring Agency Code

15. Supplementary Notes

16. Abstract

An analysis of different types of electromagnetic pumps for pumping lithium through the reactor (primary) loop of a Rankine cycle space power system has been completed. Five basic types of pumps were analyzed and screened, including a DC conduction, an AC single phase induction, a three-phase flat, an annular linear, and a helical induction design. A sixth design, which is a modification of the three-phase helical induction design but with fluid entrance and exit from the same end of the pump, was selected by NASA for the detail design study. The specific application required a pump capable of 30 lb/sec flow rate, and a 20 psi developed head, with 2100° F lithium. The pump which has resulted from the design work is approximately 50 in. long, 16 in. in diameter, weighs 1000 lb, and has an overall efficiency of 16 percent.

17. Key Words (Suggested by Author(s))	18. Distribution Statement
Nuclear power Pump Lithium	Unclassified - unlimited

19. Security Classif. (of this report)	20. Security Classif. (of this page)	21. No. of Pages	22. Price*
Unclassified	Unclassified	123	$3.00

*For sale by the Clearinghouse for Federal Scientific and Technical Information Springfield, Virginia 22151

FOREWORD

The work described herein was performed by the General Electric Missile and Space Division under NASA contract NAS 3-10604. The objective was to conduct an analytical design study program to design a flight type electromagnetic (EM) pump for possible use as a primary loop circulating pump in Rankine cycle space electric power systems. A. H. Powell and G. E. Diedrich, Nuclear Systems Programs, administered the program for the General Electric Company. The principal contributors to the program were J. W. Gahan, pump analysis and design, J. S. Longo, mechanical analysis, P. T. Pileggi, winding and insulation system and stator design, and R. G. Rhudy, pump analysis and design; all are members of the Large Generator and Motor Department. J. P. Couch of the Lewis Research Center, Space Power Systems Division, was the NASA Project Manager for the program. The report was originally issued as General Electric report GESP-337.

TABLE OF CONTENTS

LIST OF ILLUSTRATIONS

LIST OF ILLUSTRATIONS (Continued)

LIST OF TABLES

NOMENCLATURE

Units are not indicated in this tabulation since relationships used are valid in any consistent system of units. Units are indicated in the text where numerical values are given in the report.

A	area
B	magnetic induction (magnetic flux density)
c	length of fluid passage in duct
C_p	specific heat
D_h	hydraulic diameter
g	length of magnetic gap; gravitational acceleration
h	hydraulic loss factor as a number of velocity heads
I_1	phase current
I_L	line current
N_H	Hartmann number
N_R	Reynolds number
P	pressure
q	heat flow rate
Q	fluid flow rate
R	resistance (electrical)
s	slip
T ($\triangle$T)	temperature (change in temperature)
v	velocity of fluid
V_1	phase voltage
V_L	line voltage
KW	power (kilowatts)
X	reactance

δ	hydraulic friction factor
μ	fluid viscosity
ρ	electrical resistivity of fluid
σ	weight density of fluid

Subscripts

c	pertaining to stator can or coolant in heat exchanger
d	pertaining to the duct
f	pertaining to the fluid
g	pertaining to the magnetic gap
h	hydraulic, harmonic
i	pertaining to magnetic iron
m	pertaining to magnetic path, magnetization or mutual
ti	pertaining to thermal insulation
1	pertaining to the stator winding or duct wrapper
2	pertaining to the helical duct

I. SUMMARY

The General Electric Company, under Contract NAS 3-10604 to the National Aeronautics and Space Administration, has completed a design study program to determine the optimum design and related details of an electromagnetic pump for use as a primary loop circulating pump in a space electric powerplant. A specific application rated at 30 lb/sec flow rate, 20 psi developed head, 2100°F lithium was considered.

For this specific primary loop application it was not immediately obvious which type of pump would be most suitable. Therefore, the design study program was initiated and involved two major tasks:

Task 1. Preliminary design of several types of EM pumps for the primary loop application.

Task 2. Selection of most suitable type and final detailed design of the selected type.

Five types were considered in Task 1, including a DC conduction, AC single phase induction, a three-phase, flat linear induction, annular linear induction, and helical induction design. Based on a detailed evaluation and comparison of each of these types, factoring in reliability, efficiency, weight and fabricability, the three-phase helical induction EM pump was selected for the detailed design (Task 2) for this specific primary loop application. This pump type is extremely reliable, has reasonable weight, relatively high efficiency and overall proven feasibility and performance. Several concept variations and arrangements for the basic helical EM pump were considered and evaluated. Efficiency was optimized as far as possible.

Tne specific design established consists of a canned, hermetically sealed stator filled with argon gas as a heat transfer medium, and a duct with center return flow. The duct will operate in a vacuum environment isolated from the stator region by a thin metal can in the stator bore. The pump is designed for operation from a 25 Hz power supply. At approximately 120V it will produce rated output of 30 lb/sec, 20 psi, with 2100°F lithium. The pump is capable of operating continuously at its rated point. It is also capable of operation over a range of lithium input temperatures from 1900°F to 2200°F and a range of flow rates at developed pressures, from 10 lb/sec at 40 psi to 35 lb/sec at 10 psi. The final design is based upon an inlet pressure of 20 psia.

The design utilizes high temperature structural, electrical, magnetic and insulation materials to permit operation of the complete pump at environment temperatures above 800°F. The electromagnetic stator and center magnetic core are cooled with NaK at 800°F and are designed to operate at temperatures up to 1200°F hot spot through the use of nickel-clad silver wire with high temperature brazed joints, Hiperco 27 magnetic material, and a completely inorganic electrical insulation system. The duct can handle lithium up to 2200°F and is made of T-111 refractory metal alloy.

Design layouts and performance characteristics of each type of EM pump considered in Task 1 are presented. A description of the final detailed design as well as many of the detailed calculations, plus discussion of the performance and several design parameters are also included. The final pump is approximately 50" long and 16" in diameter. It will weigh about 1000 lb, and will have an overall efficiency of 16%.

II. INTRODUCTION

An extensive research program investigating all types of EM pumps for several different space applications was conducted with results reported in Reference 1. A further detailed design study program to establish a practical, optimum,helical type EM pump design for use as a Boiler Feed Pump in a space power system was conducted with the results reported in Reference 2. Such a pump is now being developed and built under Contract NAS 3-9422.

In addition, many commercial EM pumps have been developed, designed and built for liquid metal test facility loops and sodium cooled nuclear powerplants. All these pumps have exhibited excellent reliability and performance. Extensive development work has also been done on high temperature materials for use in space applications such as EM pumps, as reported in References 3 through 7.

Based on this background it is feasible to consider the use of an EM pump for the primary loop circulating pump in a Rankine cycle, space electric power system.

A comprehensive analytical design study to establish the specific EM pump design for a primary loop application was conducted. Pump design specifications included:

	Design Point	Off-Design Range
Fluid Temperature, °F	2100	1900 - 2200
Lithium Flow Rate, lb/sec	30	10 - 35
Pressure Rise, psi	20	40 - 10
Inlet Pressure, psia	20	20 - 30
NaK Coolant Temperature, °F	800	700 - 900

Material requirements include:

Duct	- T-111 Alloy
Magnetic Material	- Hiperco 27
Conductor Material	- Nickel-clad silver (20% area is Ni)
Electrical Ground Insulation	- High Purity, 99.5% Alumina
Interlaminar Insulation	- Plasma Sprayed Alumina

To determine the best design within these requirements it was necessary to first establish the most suitable type of EM pump for this specific application. As a result the design study was divided into two separate tasks as follows:

Task 1. Preliminary design of several EM pump types, including helical induction, flat linear induction, annular linear induction, direct current and single phase induction.

Task 2. Selection of most suitable type after review of all data and detailed design of the preferred type of pump.

To prepare a preliminary design of each EM pump type which represents the best balance of design (considering reliability, efficiency and weight) several hundred design variations were considered and evaluated. A limited number of preliminary design layout drawings were also prepared. The best preliminary designs were compared, and from these the most suitable type was selected for detailed design. The design work included comprehensive electrical, mechanical, thermal, and hydraulic analysis of the final design, selection of the materials, and preparation of final design layout drawings which can be used as a basis for manufacturing drawings.

III. PRELIMINARY DESIGN CONCEPTS

During the initial design phase several types of EM pumps, all with fluid inlet and outlet at opposite ends of the pump, were considered for the primary loop application. Preliminary designs were established and performance was calculated for each type. These were carefully compared to aid in selecting the preferred type for final detailed design and optimization. The specific types considered, which will be discussed in some detail, were:

A. Three-Phase Induction Pumps
   1. Helical Induction
   2. Flat Linear Induction
   3. Annular Linear Induction

B. D.C. Conduction Pump

C. Single-Phase Induction

A. THREE-PHASE INDUCTION PUMPS

The principal design guides used to establish the most optimum preliminary design for all three-phase induction pumps are as follows:

1. Allowable design stress in the T-111 duct is 3000 psi, at the maximum temperature of 2200°F.
2. The hydraulic loss should be less than 6 psi (30 percent of the developed head).
3. Average temperature rise of the winding should be kept under 275°F; closer to 200°F if possible for improved reliability

and performance.

4. Hot spot temperature rise of the winding should be kept under 400°F; closer to 300°F if possible for improved reliability and performance.

5. Efficiency and reliability are the principal considerations; weight is important but not quite as critical. There is naturally a judgment factor as to the relative degree of importance that is attached to these items. In general, an attempt was made to optimize efficiency and maximize reliability (which includes manufacturing producibility of the pump). In the final comparison, weight was factored in quantitatively by a weight-power trade off factor of 100 lb/kW input.

6. Initial calculations were based on conductor resistivity in the range of 2.13 - 2.22 $\mu\Omega$ in. This turned out to be too optimistic based on calculated winding temperature rise and NaK coolant temperature, but was suitable for relative comparison purposes. Final calculations were made with a resistivity of 2.32 $\mu\Omega$ in. which is the value for nickel-clad silver wire at 1050°F average temperature.

7. Thermal insulation surrounding the duct to have a thickness of 0.180 in.

8. To maximize efficiency and keep winding temperature rise low, current densities should be kept less than 3000 A/in^2.

1. Three-Phase Helical Induction

Performance calculations were made for a variety of designs for the helical induction EM pump. Important parameters such as frequency, fluid velocity, stator bore diameter and length, "slip," etc were varied over wide ranges to establish preferred values. This resulted in two specific preliminary designs for the helical induction EM pump which were considered to be the best for comparison purposes. One design was for 60 Hz; the other for 25 Hz. The 25 Hz design has a little better performance and is a little shorter, but has a larger diameter and is a little heavier overall. However, a significant advantage of the 25 Hz is that it has a larger bore diameter, and hence lends itself better to a center return flow design. This allows the inlet and outlet connections to be made at the same end of the pump. This means the stator could be removed from the duct without cutting the T-111 primary loop, which is a very desirable feature. In addition, thermal stresses are reduced due to the unrestrained axial thermal expansion of the duct. A center return flow pipe cannot be incorporated into the smaller diameter 60 Hz design.

Figures 1 and 2 illustrate the 25 Hz and 60 Hz preliminary helical designs respectively. Performance characteristics for these two designs are shown in Table I. Performance curves over a range of voltages and frequencies are presented in Figures 3, 4, 5 and 6.

The helical EM pump has many desirable features, including high reliability, demonstrated performance in land and marine installations, and good efficiency as compared to other EM types of pumps. It tends to be a little larger and heavier than some of the other types, but

some improvement in weight can be realized at the expense of complications in manufacture. The helical pump is thus very promising for this application.

2. Flat Linear Induction

A variety of designs for a flat linear induction EM pump were considered and evaluated. A parametric analysis and performance calculations were made over wide ranges for many of the variables which affect performance. The most promising preliminary design for a flat EM pump was established and is illustrated in Figure 7. Its performance characteristics are shown in Table 2. Performance curves over a range of voltages and frequencies are plotted in Figures 8 and 9. The efficiency of the flat EM pump is greatly affected by the duct wall thickness. The performance characteristics reported are based on a 0.04 in. thick duct wall which is about the minimum practical value. At this thickness the efficiency is not significantly better than the other types of pumps.

Although the electromagnetics of a flat EM pump are utilized more effectively than the other polyphase types, the overall weight is more because of the additional structural reinforcement required to support the flat duct. The flat duct is not self-supporting like the cylindrical duct geometries, but is backed up by the flat stators for support. Hence the flat duct is not an ideal pressure vessel, which is one of the most limiting features of the flat pump.

However, because of its good calculated performance, ease of stator and winding design and demonstrated operating experience in

other applications, it is a candidate for this (primary loop) application and requires careful consideration and comparison with the other types.

3. Annular Linear Induction

A large variety of designs were also analyzed for the annular linear induction type of EM pump. The best preliminary design established is illustrated in Figure 10. Performance characteristics for this design are listed in Table 3, and performance curves for a range of voltages and frequencies are shown in Figures 11 and 12.

The annular pump is lightest in weight and has the simplest duct. Its stator, however, involves a considerable number of unknowns and reliability risks. It has the most complicated stator construction and thus presents additional fabrication unknowns which must be factored into the comparison with other types. On an efficiency per pound basis it appears slightly better than the other polyphase types.

B. DC CONDUCTION PUMP

The DC conduction pump has been studied by many investigators, and analyses of performance of such pumps have been published in several references (refer to 1, 8 and 9). The analyses given in Reference 1 have been programmed for computer solution, and the design calculations reported here were generated by the use of this program.

The DC conduction pump configuration evaluated for the primary coolant loop application is similar to that illustrated in Figure 13. Performance calculations have been made for designs using 0.5, 1, 1.5, 2, and 2.5 turns of the series exciting winding. The designs having

an integral number of turns are assumed to be fully compensated, and those having a non-integral number of turns are uncompensated. Approximate "optimum designs" were derived for each number of turns. The principal dimensions and performance characteristics for the best preliminary design (1.5 turns) are shown in Table 4. Significant design guides used in the selection of various design parameters are:

1. The flux density in the magnet is 15.5 kilogauss.
2. The current density in the series winding is 6,000 A/in^2, and the resistivity of the conductor is 2.22 $\mu\Omega$in.
3. The duct wall thickness is 0.05 in.
4. The thermal insulation on either side of the duct is 0.125 in.
5. A total of three insulating flow splitters is used at either end of the duct to reduce the magnitude of the current fringing from the electrodes into the liquid metal outside the pumping region.

The data of Table 4 indicate an efficiency of 19 percent, for the pump having 1-1/2 turns in the exciting winding. Weight varies directly with the number of turns in the exciting winding. Approximately the same current is required for each design considered. The gap flux density is least for the half turn design, increasing with the number of turns for the other designs considered.

As is usual in such comparisons of different types of EM pumps, the efficiency for a DC pump is higher than that calculated for other pump types. The negative features of the conduction pumps are associated principally with the conduction path. These include the following:

1. The joint between the exciting winding and the duct poses an extremely difficult fabrication problem. The attainment of attractive efficiency requires the use of a material of high electrical conductivity for the exciting winding while the duct material must be a refractory metal (T-111 alloy). The duct temperature exceeds the melting point of attractive conductor materials. Thus two choices are available. Either an inferior conducting material is used for the series winding, with a serious reduction in efficiency, or a good conductor is used for the exciting winding, and the joint to the duct material is cooled. A satisfactory solution to this problem is not presently available.

2. Means of limiting fringing current at the duct ends are necessary to the attainment of attractive efficiency. Either insulating flow splitters at the entry and exit of the duct (see Figure 13) or several separate entry and exit flow passages in parallel connecting to the duct appear to be appropriate. While these constructions are believed to be feasible, they complicate the duct and introduce stress concentrations which tend to reduce duct reliability.

3. The current and voltage combination required (approximately 20,000 amperes and 1 volt) is completely incompatible with a lightweight, efficient, and easily controllable power conditioning system.

In summary, the DC conduction EM pump remains attractive in theory and concept, but very unattractive in practice and is considered much

less promising for the primary coolant loop application than the AC induction types of pumps.

C. SINGLE PHASE INDUCTION

The single phase induction electromagnetic pump was studied by Watt (Reference 19) in 1953. Verkamp and Rhudy (Reference 1) conceived several modified forms of the configuration proposed by Watt and reported calculated performance data for a pump of this type in the primary coolant loop application in a space power system. A calculated efficiency of 8 percent was reported for a rating of 40 lb/sec, 6 psi, lithium at 1700°F. Schwirian (Reference 20) performed an analysis of the performance of single phase induction pumps of the types described in Reference 1. He reports a calculated efficiency of about 14 percent for a rating of 10.3 lb/sec, 14.5 psi, lithium at 1200°F. However, he neglected losses due to current in the fluid and duct walls outside the pumping region, assuming that they could be eliminated by careful design. This does not appear feasible.

A single phase induction pump configuration is illustrated in Figure 14.

Performance calculations have been made for a variety of designs of the general type illustrated in Figure 14 for the primary coolant pump rating of 30 lb/sec, 20 psi, 2100°F lithium. Preliminary "optimum designs" were derived for five frequencies: 15, 30, 60, 120, and 240 Hz. The principal dimensions and performance characteristics for the best preliminary design (60 Hz) are shown in Table 5. Significant design guides used in the selection of various design parameters are:

1. The peak flux density in the magnetic core is 16.8 kilogauss.

2. The current density in the exciting coil is 4000 A/in^2.

3. The resistivity of the exciting coil conduction is 2.22 $\mu\Omega$ in. which is based on an average winding temperature of 1000°F.

4. The allowable design stress in the duct wall is 3000 psi.

5. The geometric parameter for the permeance of the exciting coil is 2 $in./in^2$.

6. Insulating baffles are used in the headers at either end of the annular duct. The resistance of each of the headers (with their insulating baffles) is 0.0005 ohms.

7. The thermal insulation surrounding the duct has a thickness of 0.125 in.

8. The hydraulic loss in all units is 5 psi.

The data of Table 5 indicates an efficiency of 6.4 percent. In general the efficiency does not vary significantly with frequency. Size and weight decrease rapidly with increasing frequency. The power loss in the headers at the ends of the duct is of major proportions, on the order of about 35 kW. Each header constitutes a conducting loop around the flux carrying core. If power loss in the header could be eliminated, the efficiencies would approach 15 percent. The calculations are based on a resistance of 0.0005 ohms through the headers. While this figure is somewhat arbitrary, it is believed to be representative of the resistance attainable in a practical design.

The most significant advantages and disadvantages of the single phase induction pump are as follows:

Advantages:

1. The configuration is compact, and pump weight is reasonable.
2. The duct is cylindrical in form and may be made self-supporting with respect to internal pressure.
3. The exciting coil is simple and compact, relatively remote from the hot duct, and well suited to liquid cooling.

Disadvantages:

1. The pump is at a very early stage of development. Performance has not been demonstrated.
2. The duct is extremely complex in form, requiring a large number of hydraulic connections and internal insulated baffles (or the equivalent) to control the electrical losses.
3. The developed pressure is pulsating, with a peak value approximating twice the average value and a pulsation frequency of twice the power supply frequency.
4. The pump constitutes a single phase load; hence, is less attractive than a polyphase load, from a power supply and power conditioning view point in a space power system.
5. The efficiency is considerably less than that for other types of EM pumps.

In summary, while the single phase induction EM pump has some attractive features, it remains much less promising for the primary coolant loop application than some of the more highly developed polyphase induction pumps.

D. OVERALL COMPARISON AND EVALUATION

Evaluation of the single phase and DC types of EM pumps indicates that these are less attractive than the polyphase induction types (helical, flat and annular) for the primary loop application. Therefore, these two types were eliminated from further consideration. Based on this, subsequent comparison and evaluation was restricted to the helical, flat,and annular types of EM pump. The principal factors considered in this evaluation and comparison include:

1. Reliability
2. Efficiency - power input
3. Producibility
4. Size and weight

Detailed comparison of the three polyphase types actually results in relatively small differences of efficiency, size and weight. Reliability is good in all types because of no moving parts and opportunity for conservative insulation and conductor arrangements. There are, however, considerable differences in producibility or ease of manufacture. In evaluating weight and power consumption, a power input-to-weight tradeoff of 100 lb/kW input was used. If in the light of current system design studies, this trade off is considered low, this would tend to favor higher efficiency, rather than lighter actual weight.

Tables 6, 7, and 8 present in detail the summary comparison of the helical, flat and annular pump configurations. Table 9 gives an indication of how the different pump types would respond to significant changes in rating. As is normal in comparisons of this type, no one single solution is optimum. It is impossible to combine the advantages

of each into one concept and arrive at an obvious, clear-cut solution. The flat pump offers considerable ease of stator and winding design, but has a structural weakness in its flat duct which has to be supported by the stator. It also is heaviest.

The annular type has a simple duct and lowest weight, but an extremely difficult stator to build, with several unknowns and risks. The helical pump is similar to the boiler feed pump previously designed for space application and currently in hardware development (Reference 2). The 25 Hz helical pump has the very desirable feature of permitting a center return flow although it is a little heavier.

In overall rating, it is felt that the helical pump has the highest probability of success for the given design specifications and this specific application.

Based on this detailed comparison, the evaluation and the relative importance of some of the qualitative factors (such as center return flow), the 25 Hz three-phase helical induction EM pump was selected for conducting detailed design and analysis for this primary loop application.

IV. DESCRIPTION - FINAL DESIGN

A. PRINCIPLE OF OPERATION

In all EM pumps a body force is produced on a conducting fluid by the interaction of an electric current and the resulting magnetic field in the fluid, with the magnetic field of the stator. This body force results in a pressure rise in the fluid as it passes from the inlet to the outlet of the EM pump, and is analogous to the familiar fundamental principle of force on a current carrying conductor in a magnetic field, the operating principle of many common electromagnetic devices.

The polyphase helical induction EM pump operates in a manner that is similar to a polyphase induction motor. The pump contains an electromagnetic stator assembly and a duct assembly in the stator bore. When power is applied to the three phase stator winding a "revolving" magnetic field is produced in the stator bore. This magnetic field induces voltage in the conducting fluid contained in the duct, and as a result of this induced voltage, currents will flow in the fluid. These currents set up a magnetic field which interacts with the magnetic field of the stator to produce a body force on the fluid, causing it to move through the duct thereby developing pressure. The pressure gradient at any point in the fluid is proportional to the product of magnetic field strength and the component of current density perpendicular to the magnetic field strength. The total pressure rise developed by the pump is the integral of this pressure gradient over the axial length of flow passages in the pump duct.

B. GENERAL ARRANGEMENT

The general arrangement of the final helical EM pump design with center return flow is shown in Figure 15. This design layout is for a basic rating of 30 lb/sec, 20 psi, 2100°F lithium, three phase, 25 Hz, 120 volts, with NaK coolant having an inlet temperature of 800°F. The major parts comprising this pump are: heat exchanger and shell, stator, pump duct with center return, thermal insulation, and center core iron.

In the configuration shown in Figure 15, the liquid metal enters the pump duct through the 4.26 inch inlet pipe into a short annular region, then into and through the helical passage where pressure is developed by the electromagnetic body force on the fluid. After leaving the helical passage the fluid flows back through the center return leaving the pump through a 4.26 inch outlet pipe at the same end it entered. Low fluid velocity is maintained near the pump entrance where the net positive suction head (NPSH) is lowest.

The pump is cooled by means of a heat exchanger around the periphery of the pump frame or shell. The heat exchanger consists of a machined helical passage, with an inlet pipe at each end and an outlet pipe at the center of the pump frame region adjacent to the stator. Heat is conducted from the windings through the stator core to the frame where the heat is removed by circulation of liquid metal coolant through the heat exchanger.

The stator core and windings are completely enclosed and sealed by the frame, end shields, and a thin can or liner inside the stator bore. This enclosed stator region is filled with an inert gas to pre-

clude oxidation and facilitate heat transfer between the windings and the stator laminations to the frame. Electrical power is transmitted to the stator windings through hermetic lead seals in the pump frame.

The region between the duct and the stator can includes thermal insulation consisting of several layers of rippled metallic foil. This space between the duct and stator can is designed for operation in a vacuum environment.

C. STATOR ASSEMBLY

The stator consists of a laminated punching stack and form-wound coils arranged to form a two-pole magnetic field revolving at 25 revolutions per second, three phase power. Selection and evaluation of the specific electrical, magnetic and insulating materials for the stator assembly were based primarily on prior development work done under government contract. The results of this work and the data generated are contained in References 3 through 7.

The punching stack consists of magnetic laminations clamped tightly together, which provide a low reluctance path for the magnetic flux as in a conventional induction motor stator. The strength requirements for the stator laminations are not severe. The main requirement is that the material maintain its highly magnetic characteristics at its operating temperature which is between 800 and 1000°F. Therefore, the magnetic material selected for these laminations is Hiperco 27 approximately 0.025 in. thick. For the conditions of operation, and in this lamination thickness, Hiperco 27 has excellent magnetic characteristics, good thermal conductivity and reasonably

low loss. Each lamination contains 36 slots for the stator winding.

Interlaminar insulation is provided by a plasma sprayed alumina coating on each lamination. This coating will be approximately 0.001 to 0.002 in. thick.

Significant stator core dimensional parameters include:

Core length	15 in.
Bore diameter (punching)	9.20 in.
Outside diameter (punching)	14.85 in.
Slot depth	1.885 in.
Slot width	0.440 in.

The stator laminations are held together by eight "building" bars of rectangular cross section spaced uniformly around the outer periphery of the punching stack and welded at each end to a welding ring to form a tightly compressed stack of laminations. The stator core has an interference fit at its outer periphery with the pump frame thereby insuring good heat transfer from the stator to the heat exchanger. In addition, two dowel pins are inserted through the frame into one of the welding rings to properly position the stator core.

Form wound coils are inserted in the 36 slots of the stator core. The conductor material is nickel-clad silver wire with a cross section including an area of 20 percent nickel. This conductor material has an acceptable electrical conductivity at the operating temperature range of 1000°F to 1200°F. The electrical conductivity of the nickel clad silver is one of the major factors contributing to the relatively high pump efficiency. Other considerations given to selection of conductor material for

high temperature operation include thermal conductivity, physical strength, creep and rupture strength, resistance to oxidation both during processing and normal operation, thermal diffusion stability, and the ease with which joint fabrication and other manufacturing processing can be accomplished. The nickel clad silver conductor appears to best meet the overall requirements for long time reliability. In the future, additional data on thermal cycling requirements for high temperature operation, creep and rupture fatigue properties of the nickel-silver combination should be reappraised in the light of all requirements.

The ground, turn, and phase insulation for the slot or stator core region will consist of high purity (99.570+) alumina ceramic strips of suitable width and thickness. The arrangement and assembly of the ceramic ground, turn, and phase insulation is shown in the end view, Section "A-A", of the general arrangement drawing, Figure 15.

The turn and phase insulation in the end turn region consists of layers of "S" glass tape, 0.005 in. thick, "C" weave, with a high temperature finish. The 1" wide tape is a heat cleaned material (the original binder is removed by the heating) so it can be subsequently used up to 1400°F. It is thus compatible with the ceramic slot liners and conductor separators.

Each coil consists of three turns of a group of six wires, each wire 0.080 in. x 0.175 in. rectangular shape, with a 2/3 pitch or 1 to 13 slot throw. The coils are inserted into the stator core to form a double layer arrangement, also shown in Figure 15. The 36 stator coils are connected three phase (circuit wye) with 36 turns in series per phase.

Radial and tangential coil end movement due to electromagnetic forces is precluded by tying each lower or outer coil side onto a 3/16 in. section diameter stainless steel ring with "S" glass tape. Movement of each of the total coil ends enmasse is precluded by three equally spaced bearing surface pads which radially restrain and position the end turns. The bearing surface pads are shown on Figure 15.

D. HEAT EXCHANGER AND FRAME

Surrounding the stator core is the pump heat exchanger and frame. Liquid metal coolant, NaK, is circulated through the helical passage in the heat exchanger to remove heat conducted from the windings through the stator core.

The material selected for the pump frame and heat exchanger is Hastelloy B. This material has adequate strength at operating temperature, is a satisfactory containment material for the liquid coolant (NaK) in the heat exchanger, and comes quite close to matching the thermal coefficient of expansion of the Hiperco 27 stator core. By matching the thermal expansion of the Hiperco 27 stator core, the interference fit between the heat exchanger and the core is easily maintained, providing good heat transfer between the core and heat exchanger at operating temperature. Beyond the ends of the heat exchanger, the pump frame material is from Inconel. The end shields and stator "can" in the stator bore are also Inconel to simplify fabrication and joining. The heat exchanger, frame, end shields, and stator "can" provide all welded construction and form a completely sealed envelope around the stator coils and iron. The only penetrations through this envelope are the hermetic lead seals to transmit power to the stator windings, thermocouple wells to provide means of

monitoring stator winding temperature, and an evacuation plug to provide a means of leak testing the unit, evacuating the stator region and filling with inert gas. All these penetrations are then completely sealed by brazed or welded joints.

E. DUCT

The T-111 duct design is shown in overall layout in Figure 15. The axial length of the helical duct for this design is approximately 18 inches with the overall length including inlet/outlet connector being about 35 inches. The outside diameter of the duct is 8.8 inches. The machined helix has a total lead of 6.4 inches, with five machined passages in parallel. Cross sectional dimensions of the machined helical passage are also shown in Figure 15. The duct is entirely self-supporting with the inlet/outlet connections at the same end of the pump.

F. CENTER CORE AND CORE HEAT EXCHANGER

Enclosed between the helical flow passage and the center return pipe is a center iron core. This center iron core consists of magnetic laminations (washers) of Hiperco 27 having the same thickness and same interlaminar insulation as the stator core laminations. These laminations are held together in a tight stack and positioned by a key and ring at each end.

The center core iron is thermally insulated, on the outside, and cooled by circulating NaK through a stainless steel heat exchanger which is in intimate contact with the core iron inside diameter. The heat exchanger consists of two concentric cylinders with separating walls placed 180° apart between the cylindrical walls so as to direct the flow

down approximately one half of the cylindrical surface and back through the remaining half. Both inlet and outlet connections are located at the same end between the pump inlet and outlet connections. The core and core heat exchanger are essentially self-supporting by means of the loop connections and input end attachments.

G. THERMAL INSULATION

The thermal insulation between the duct and stator "can" consists of several layers of laminated strips of Cb-1Zr metallic foil. These strips are approximately 0.5 in. wide by 0.002 in. thick with "ripples" approximately 0.010 in. to 0.015 in. deep.

The thermal insulation is applied directly to the duct O.D. and thus exposed to a vacuum environment in service. Hence, these layers of foil serve as radiation barriers to the heat load from the duct. Contact between layers is kept to a minimum to minimize the heat load by conduction. Similar thermal insulation is also applied between the duct I.D. and center core O.D., and between the center core heat exchanger O.D. and center return pipe I.D.

V. DESIGN EVALUATION - FINAL DESIGN

A. DESIGN PERFORMANCE AND CHARACTERISTICS

The operating performance of the pump is calculated through the use of an equivalent circuit as explained in Section VI, Part A, the solution of which has been programmed for a digital computer. This equivalent circuit is shown in Figure 16. Performance curves, shown in Figures 17 through 22, and tabulated values in Tables 10 and 11 indicate overall calculated performance characteristics for the final design. Additional calculated results and design characteristics are presented in the details in Tables 12, 13, 14, 15 and 16.

In addition to these results, certain operational limits and conditions are necessary to insure satisfactory operation throughout the pump's life. The principal limits are as follows:

1.	Duct and fluid temperature	2200°F maximum
2.	Stator coolant flow rate - NaK	2 lb/sec minimum
3.	Stator coolant inlet temperature - NaK	800°F maximum
4.	Duct pressure	70 psia maximum
5.	Stator cavity pressure at room temperature	7 to 9 psia
6.	Suction pressure	20 psia minimum

The limitation on duct and fluid temperature and pressure is primarily one of strength. The duct was designed mechanically to safely withstand pressures up to 70 psia at 2200°F maximum. From an operational standpoint the pump is designed for continuous operation at 2100°F and rated flow and developed pressure. It is capable of operation for a limited time over the off-design point range of flow

rate and pressure given in the pump specifications and at temperatures up to 2200°F.

Pump losses are divided into four parts:

1. Winding I^2R (power)
2. Fluid I^2R (Slip)
3. Iron-hysteresis and eddy current.
4. Bore seal (can) and duct eddy current (I^2R equivalent) plus insulation (small).

The limitation on stator coolant flow rate and temperature is based on the heat exchanger design and a reasonable limit of the winding temperature to 1200°F maximum hot spot and 1050°F average. The winding and insulation system is capable of temperatures in excess of these amounts. However, both performance and life will be affected. All calculations are based on an electrical resistivity of the conductor material at an average temperature of 1050°F. Average temperatures above this will cause increased winding resistance, I^2R (power) losses in the stator windings, and lower efficiency.

The limitation on stator cavity pressure depends on both mechanical and electrical considerations. The maximum pressure of 9 psia at room temperature is a mechanical limitation. At operating temperature the pressure in the winding cavity increases by a factor of almost three. To minimize weight, the frame structure has been mechanically designed for maximum internal pressures of about 30 psia. Hence, at room temperature internal winding cavity pressure must be limited to about 9 psia. It is unreasonable to add weight to the frame to design it for unnecessarily high pressures. The lower limit of 7 psia is based on

electrical considerations. Because of reduced arc-over voltage of the winding and insulation system at pressures below about 7 psia, it is recommended that this be the minimum winding cavity pressure at room temperature to provide adequate margin for electrical tests during manufacture. This will result in a pressure of about 6 psi above atmospheric, at operating temperature.

The limitation on suction pressure is based on the design specifications and cavitation considerations, using the criterion of requiring an NPSH of at least two velocity heads at entrance to the pumping section. This criterion is explored in Reference 1 and appears to be reasonably conservative.

B. DISCUSSION OF SIGNIFICANT PARAMETERS

There are several significant parameters which were varied in this analytical study to determine the final design which represents a balance of optimum efficiency, maximum reliability, minimum weight and production feasibility. The most important parameters once a set of materials and the basic concept have been selected, are (1) fluid passage cross sectional geometry, (2) duct wall thicknesses and total magnetic gap, (3) frequency, (4) duct, fluid passage and stator diameters, (5) duct and stator length, and (6) velocity and slip (the difference in rotational speed of fluid and magnetic field) as determined by the interrelation between frequency, fluid passage geometry, and duct diameter. All of these parameters were varied over a considerable range in this design study. Several hundred computer runs were made to cover a multitude of combinations of these variables.

Fundamentally a helical induction EM pump is a relatively low flux density machine due to its large magnetic (air) gap as compared with conventional induction motors. Large magnetizing currents become necessary to establish the required flux levels in the gap which in turn result in relatively low power factors. Hence, it is desirable to make the gap between the stator core and center iron structure as small as possible by keeping the thermal insulation thin, the duct walls thin and the fluid passage height small. Thin duct walls are also desirable to reduce I^2R losses in the duct material since these are directly proportional to duct thickness.

Fluid velocity and slip are very important parameters and are established by the fluid passage cross section, power frequency, and duct diameter. Various combinations of these parameters must be investigated to determine optimum values.

In a study such as this to determine the best design which meets certain specification requirements, it becomes quite clear very early in the design phase that no sharp optimum exists. Because of the interrelation among so many variables, there are several designs which meet the requirements, any one of which could be considered optimum by certain individuals. Hence, selection of the final design involves a considerable amount of judgment and experience.

For example, the optimum frequency for these designs occurs over a range of about 20-30 Hz. Frequencies below 20 Hz require considerably larger diameters for good performance, and hence result in a much heavier pump. Frequencies above 30 Hz can be made to have about equivalent performance but their diameter is too small to permit the preferred center return flow design.

It is also desirable to operate induction EM pumps at relatively high fluid velocities and low slip for efficient operation. However, velocity is limited by hydraulic loss and NPSH. In addition, as the slip decreases the efficiency at the design point eventually goes through a maximum, since fluid (slip) loss decreases while winding and duct I^2R loss increases with decreasing slip.

Current density, another important design characteristic since it directly affects winding temperature, goes through a minimum as the slip is decreased due to the load component of current decreasing while the magnetizing component is increasing. It is desirable to select a velocity, slip and corresponding flow passage geometry (cross section and diameter) to give peak efficiency and minimum winding current density at the design point. Since these do not occur at precisely the same point the final design must provide the proper balance between efficiency and current density factoring in hydraulic loss and NPSH.

One other item which determines the NaK cooling temperature is the nickel clad silver conductors. Nickel has a Curie point of about 675°F. Below this temperature the nickel sheath over the silver wire is magnetic. If the conductors in the stator iron area are not above 675°F, the pump performance is adversely affected and, in fact, could not be reliably predicted. Therefore, the coolant temperature should be at least 600°F for the winding temperature to be at or above 675°F.

VI. APPENDIX - ANALYSIS DETAILS & FINAL DESIGN

A. PERFORMANCE CALCULATIONS - EQUIVALENT ELECTRICAL CIRCUIT

Generalized expressions for power output, losses, pump efficiency, developed pressure, and other basic characteristics are developed and available in several references, i.e., References 1, 8 and 9. To design and analyze a specific EM pump these basic expressions have to be related to the stator structure, windings and detailed dimensional data for the particular configuration being considered. In addition other items neglected in the generalized expressions, such as end effects, flux fringing, iron losses, hydraulic losses, etc., must be properly taken into account. This is most readily done through the use of an equivalent electrical circuit for the EM pump which is the same approach used in induction motor design.

Equivalent Circuit

The equivalent circuit used in this design study for each phase of the three phase helical induction EM pump is shown in Figure 16. Its derivation and solution are analogous to that for an induction motor as presented in several classical texts such as Reference 10. The solution of this circuit is used to determine the complete performance characteristics for any specific helical induction EM pump. The basic equations as applied to any induction EM pump are discussed in References 1 and 8. Equivalent circuit parameters are calculated in terms of the geometry of the specific pump being analyzed. This calculation of parameters, solution of the equivalent circuit, and translation of the circuit solution into pump performance, has been programmed for calculation on a digital computer.

The complete performance prediction procedure used in the calculation of helical induction pump performance was developed during the past several years, on this program as well as on earlier programs such as the Boiler Feed EM pump. This procedure takes into account the end effects caused by imperfect end rings at the axial extremities of the pumping section; end effects caused by discontinuities in electromagnetic body force at the ends of the helical flow passages; the negative pressure gradient caused by the axial velocity of the fluid in the magnetic field; the effect of the curvature of the configuration on the magnetic field; and the principal mutual effects of the various duct wall, stator can, and fluid currents. Other refinements frequently neglected in approximate performance calculation procedures are also incorporated here. This procedure has been used in conjunction with the design of helical induction pumps, operative since 1962. Highly successful operation of these pumps confirms the validity of the performance prediction procedure.

Final Design Variations

To determine the final design for this study many design variations were run on the computer. Basic design parameters that were varied included frequency, duct and stator diameters, stator slot and winding geometry, fluid velocity, duct flow passage geometry, and stator length. Several hundred computer runs were made to determine the preferred design parameters and geometry. For the final helical EM pump design selected, the equivalent circuit parameters in Figure 16, based on computer calculations, are given in Table 17.

The parameters in the equivalent circuit use symbols defined in the Nomenclature. Two items which may require further clarification are the

leakage reactance term X_1 and the dimensionless parameter s'. The reactance X_1 consists of stator winding leakage reactance, outer duct wrapper leakage reactance, and winding harmonic leakage reactance.

The dimensionless parameter s' is a function of slip and takes into account the fact that the liquid metal is moving through the helical passage at some slip s, while the duct separators between the helical flow passages are stationary (unity slip). The current in this path flows axially through the moving fluid and the stationary separators. Hence s' can be thought of as an effective slip value for the fluid and separators in series. In addition, s' takes into account an end effect where the liquid metal enters and discharges from the helical passage.

Calculated Results

The calculated results shown in the performance curves of Figures 17 through 22, and the data in Tables 10 and 11, for the final design, were obtained using this equivalent circuit and the associated computer program. The data covers all specified "off-design" conditions of fluid temperature, flow rate, developed pressure, and frequency, in order to explore the maximum expected pump conditions.

B. HYDRAULIC ANALYSIS

The computer program for the solution of the equivalent electrical circuit and calculation of performance includes a calculation of hydraulic loss through the pump, and factors this into the calculation of overall performance. Basically, the hydraulic pressure drop through the pump duct can be expressed as,

$$P_h = 4\delta \frac{c}{D_h} \left(\frac{\sigma v^2}{2g}\right) + h \left(\frac{\sigma v^2}{2g}\right) \qquad \text{(B-1)}$$

where the first term represents the friction drop through the helical passage and the second term represents the hydraulic loss, as a number of velocity heads, in entering the helical passage, leaving the helical passage, making a 180^{o} bend into the center return pipe and passing through the center return pipe. Friction factor, δ, depends on Reynolds number and Hartman number which are determined through use of the following basic equations:

$$N_R = \frac{\sigma v D_h}{\mu} \qquad \text{(B-2)}$$

$$N_H = \frac{B_f D_h}{4\sqrt{\rho_f \frac{\mu}{g}}} \qquad \text{(B-3)}$$

The helical passage is 1.1 in. deep and has a lead of 6.4 in. with five passages in parallel and a 0.06 in. thick separator between passages, thereby making the individual flow passage 1.22 in. wide.

For the final design the significant parameters for the equations above are as follows:

D_h (inches)	1.158
B_f (kilogauss)	2.4
N_R	360,000
N_H	152
v (ft/sec) (through helix)	25.5

These data indicate that the flow through the helix is turbulent. Entering a curve of δ as a function of N_R and N_H as presented in Reference 1, one determines the friction factor in the duct to be approximately 0.0035. To account for curvature a slightly conservative value of 0.005 was used in the computer design calculations. The entrance and exit loss factor, h, was estimated as

1.5 velocity heads based on geometry and past experience with similar type pumps. The resulting net hydraulic loss at 2100°F from the duct inlet to the duct outlet, as determined by computer calculation based on equation (B-1) and used in the overall performance calculations, is as follows:

Duct Entrance Loss (psi)	0.77
Loss Through Helical Passage (psi)	2.18
Helix Exit 180° Bend Loss (psi)	1.56
Center Return Pipe Loss (psi)	0.43
Total Hydraulic Loss (psi)	4.94

This loss is shown in Table 12. An elbow and reducer, such as shown in Figure 15, and if needed at the end of the center return pipe of the duct to connect to the external loop, would add an additional small loss.

C. HEAT TRANSFER ANALYSIS

Temperature of the stator winding is a principal factor in limiting output. It is a function of the liquid metal and duct temperature, winding current density, cooling system, and the geometry and thermal characteristics of the pump structure. The temperature rise of the winding can be determined through the use of an equivalent thermal circuit. Solution of an equivalent thermal circuit for a liquid cooled helical induction pump, with a heat exchanger around the frame as in this case, has been programmed on a digital computer. The results of calculations at the design point using this program for the final pump design described in this report were as follows:

Winding Hot Spot Temperature Rise	367°F
Winding Average Temperature Rise	225°F

These results represent the temperature rise above average coolant temperature. For average NaK coolant temperatures of 825°F the actual winding temperatures thus become:

Winding Hot Spot Temperature	1192°F
Winding Average Temperature	1050°F

These results are based on assuming that the entire heat load flows through the stator core to the heat exchanger, which is conservative, since some heat will be convected or radiated from the winding end turns. The accuracy of these results is limited primarily by the accuracy of the thermal resistivities used in the computer program, especially the effective resistivity of the thermal insulation between the duct and stator, and the electrical insulation between the conductors and stator iron. These thermal resistivity values are tabulated in Section E, Design Data and Physical Properties, at the end of this Appendix. The values used are somewhat conservative.

The portion of duct and fluid loss (heat) transmitted to the stator heat exchanger consists of the stator (I^2R) losses plus the heat loss from the duct through the thermal insulation. For the design point with the liquid metal at 2100°F and an average NaK coolant temperature of 825°F the heat loss from the duct, stator losses, and total heat load to the stator heat exchanger are as follows:

Heat Source	Heat Loss, kW
Loss From Duct Through Thermal Insulation	4.27
Winding (I^2R) Losses	7.76
Iron Loss	2.0
Stator Can Loss	0.5
Total Heat Load	14.53

The total heat load transmitted to the center core heat exchanger consists of the heat from the duct thru the thermal insulation and then thru the center core (picking up any small losses in the center core) plus the heat loss from the center return pipe thru the thermal insulation.

For the same conditions as above, the heat load to the center core heat exchanger is as follows, and is shown in Table 13:

Heat Loss from duct thru thermal insulation and thru center iron core, kW	4.0
Heat Loss from center return pipe thru thermal insulation, kW	4.0
Total Heat Load to center core heat exchanger, kW	8.0

Therefore the total heat load to the NaK coolant heat exchanger system is 14.53 + 8 = 22.53 kW, and is included in the Performance Characteristics, Table 10.

The heat loads thru the thermal insulation are based on a minimum number of layers of the Cb - 1%Zr foil used as the thermal insulation. Since the environment is vacuum each layer acts, almost entirely, as a radiation barrier.

The minimum number of layers of foil to limit the radiation heat loads to the above values and the recommended number of layers are as follows:

	Minimum	Recommended
Outside duct	4 layers	8 layers
Inside duct and outside center core	3 layers	6 layers
Outside center return pipe	3 layers	6 layers

By using the recommended number of layers the heat loads will be even less than above and any possible heat loss by conduction will be

kept to a minimum. Based on these heat loads the heat exchanger requirements can be established. Typical calculation is as follows.

If the average coolant temperature desired is 825°F, then for a coolant inlet temperature of 800°F the outlet temperature must be 850°F giving a coolant temperature rise through the heat exchanger of 50°F. The required NaK coolant flow is given by:

$$Q = \frac{\frac{3413}{3600}(q_T)}{C_p \ \Delta T} \qquad \text{(C-1)}$$

where

q_T = Total heat load in kW

C_p = Specific heat of NaK in $\frac{\text{Btu}}{\text{lb } °\text{F}}$

Q = NaK coolant flow rate in lb/sec

Using a conservative value of 23 kW for the heat load, one calculates

$$Q = \frac{3413\ (23)}{(.208)(50)(3600)} = 2.1 \text{ lb/sec}$$

This is the minimum required flow for this heat load and temperature rise. For parallel flow with inlet at each end of the stator heat exchanger and outlet at the center, the recommended minimum flow is 1.05 lb/sec per half.

The 50°F NaK coolant temperature rise is approximately divided between the stator and center core heat exchangers as follows: (based on eq C-1)

$$\Delta T_{\text{(center core H.E.)}} = \frac{3413\ \ (8)}{.208(2.1)(3600)} = 17.4°\text{F}$$

$$\Delta T_{(\text{stator H.E.})} = \frac{3414\ (15)}{.208\ (2.1)\ (3600)}$$

The NaK coolant pressure drop through the stator heat exchanger is calculated as follows:

Area of coolant flow passage, $A_c = .375 \times .95 = .356\ \text{in}^2$

Hydraulic diameter, $D_{hc} = \frac{4\ (.356)}{2\ (1.325)} = .537$ in.

Velocity of coolant, $v_c = \frac{.32\ (10)}{.356} = 8.98$ ft/sec

Velocity head, $\frac{\sigma_c v_c^2}{2g} = \frac{47.6\ (8.98)^2}{64.4 \times 144} = .414$ psi

Reynolds number, $N_R = \frac{\sigma_c v_c D_{hc}}{\mu_c} = 153{,}000$

For this Reynolds number, the friction factor, δ, is approximately 0.005 which gives a pressure drop through one half the heat exchanger of

$$\Delta P = 4\delta \frac{c}{D_{hc}} \frac{\sigma_c v_c^2}{2g} = 5.58 \text{ psi}$$

The entrance and exit losses for the stator heat exchanger are approximately 2.74 psi. The loss thru the center core heat exchanger calculated in a similar manner is about 1.25 psi. Therefore, the total pressure drop thru the heat exchanger is

$$\Delta P_T = 5.58 + 2.74 + 1.25 = 9.57 \text{ psi}$$

To account for minor additional losses in the series connection between the two heat exchangers, the heat exchanger requirements can be established as a total flow of 2.1 lb/sec, at 10 psi pressure for the final design.

Also of interest is the temperature rise of the primary liquid metal, lithium, through the EM pump duct. For the final design this is calculated as follows:

$$\Delta T_f = \frac{3414\ (q_f)}{C_p\ Q_f\ (3600)}$$

where

q_f = total heat generated in duct and fluid less heat transmitted through thermal insulation.

$$q_f = kW_{d1} + kW_{d2} + kW_f + kW_h - kW_{ti}$$

$$qf = 2.48 + 1.37 + 8.15 + 1.11 - (4.27 \div 4) = 4.84\ kW$$

$$\Delta T_f = \frac{3413\ (4.84)}{.985\ (30\ X\ 3600)} = 0.155°F$$

This rise is quite insignificant compared to the 2100°F fluid temperature. Even if the heat transmitted thru the thermal insulation is ignored the temperature rise of the lithium is only .419°F which is also insignificant.

D. MECHANICAL DESIGN ANALYSIS

This section of the Appendix contains the detailed mechanical analysis and calculations required to verify the structural integrity of the helical EM pump design shown in Figure 15. References 11, 12, 13, 14, 15, and 16 were used in various parts of this analysis.

The calculations are sub-divided as follows for ease of reference:

1. Duct
    a. Outer Wrapper
    b. End Cap
    c. Intermediate Cylinder
    d. Inner Cylinder
    e. Helix
    f. Inlet/Outlet Pipes
    g. Center Core Heat Exchanger
    h. End Shields

2. Frame and Stator Heat Exchanger
    a. Internal Pressure
    b. Outer Shell - Connection End - Inconel
    c. Outer Shell - Hastelloy B
    d. End Shield - Connection End - Inconel
    e. Outer Shell - Opposite Connection End
    f. End Shield - Opposite Connection End
    g. Stator Heat Exchanger
    h. Stator Heat Exchanger Wrapper
    i. Stator Can
    j. Stator Can Welds
    k. Stator Can End Plate

The following list of symbols applies to this Appendix section only:

- c - Distance of fiber from centroid - inch
- D - $EL^3/12\ (1 - \nu^2)$ - inch-lb
- d - Diameter - inch
- E - Modulus of Elasticity - psi
- I - Moment of Inertia - $(\text{inch})^4$
- M_o - Moment at End - inch-lb/inch
- m - $1/\nu$
- P - Pressure - psi
- R, r - Radius - inch
- T - Temperature - °F
- t - Thickness - inch
- V_o - Shear Force at End - lb/inch
- α - Coefficient of thermal expansion - in/in/°F
- β - $\left[3(1 - \nu^2) / R^2t^2\right]^{1/4}$ - $(\text{inch})^{-1}$
- δ - Deflection or expansion - inch
- $\Delta\delta$ - Differential deflection or expansion - inch
- λ - Identical to β
- ν - Poisson's ratio - dimensionless
- σ - Stress - psi

Subscripts

- 1 - Refers to head
- 2 - Refers to shell
- H - Hastelloy
- h - Hoop (stress)

I - Inconel

i - Inside (radius)

ℓ - Longitudinal (stress)

o - Outside (radius)

P - Punching

r - Radial (stress)

t - Tangential (stress)

1. Duct

The duct material is T-111 alloy. At the maximum temperature of 2200°F, the value for S_m was taken as 3000 psi.

a. Outer Wrapper

(1) Primary Pressure Stress

From Reference 11, page 268 Case 1 the longitudinal membrane stress is:

$$\sigma_\ell = \frac{PR_i}{2t} = \frac{70 \times 4.30}{2 \times .101} \qquad \text{(D-1)}$$

$$\sigma_\ell = 1490 \text{ psi}$$

The hoop stress is:

$$\sigma_h = 2\sigma_\ell = 2980 \text{ psi}$$

(2) Stress Due to Shrink Fit of Wrapper Over Helix

The wrapper will be assembled over the helix with an approximate 0.002 inch radial interference fit. From Reference 11 page 268 Case 1, this radial displacement is:

$$\sigma = \frac{R}{E}(\sigma_h - \nu\sigma_\ell) \qquad \text{(D-2)}$$

and $\sigma_h = 2\sigma_\ell$ Thus,

$$\sigma = R/E\ (2 - \nu)\ \sigma_\ell$$

Substituting known values:

$$.002 = \frac{4.35 \times 1.7}{21.6 \times 10^6}\,\sigma_\ell$$

$$\sigma_\ell = 5{,}842 \text{ psi}$$

$$\sigma_h = 11{,}684 \text{ psi}$$

(3) Stress Due to Discontinuity at End Cap

From Reference 11 page 275 Case 24 the moment due to the discontinuity is:

$$M_o = \frac{\left[\frac{PR^3\lambda^2 D_2}{4D_1(1+\nu)} + \frac{2PR^2\lambda^3 Et_1 D_2}{Et_2(1-1/2\nu)\left[Et_1 + 2RD_2\lambda^3(1-\nu)\right]}\right]}{\left[2\lambda + \frac{2R\lambda^2 D_2}{D_1(1+\nu)} - \frac{\lambda Et_1}{Et_1 + 2D_2\lambda 3R(1-\nu)}\right]} \qquad \text{(D-3)}$$

where:

$$\lambda = \sqrt[4]{\frac{3(1-\nu^2)}{R^2 t^2}} = 1.9393 \text{ in.}^{-1} \qquad \text{(D-4)}$$

$$D = \frac{Et^3}{12(1-\nu^2)} \qquad \text{(D-5)}$$

$D_1 = 469{,}501$ in.-lb. ($t = .625$ in.)

$D_2 = 1{,}981$ in.-lb. ($t = .101$ in.)

Substituting known values:

$$M_o = 18.79 \text{ in-lb/in}$$

$$V_o = M_o\left[2\lambda + \frac{2R\lambda^2 D_2}{D_1(1+\nu)} - \frac{PR^3\lambda^2 D_2}{4D_1(1+\nu)}\right] \qquad \text{(D-6)}$$

$$V_o = 57.29 \text{ lb/in}$$

The stresses at the ID due to these reactions are:

Moment

$$\sigma_\ell = \frac{6\,M_o}{t^2} = +11{,}053 \text{ psi} \qquad \text{(D-7)}$$

$$\sigma_h = \frac{2\,M_o\,\lambda^2\,R}{t} = 6{,}087 \text{ psi} \qquad \text{(D-8)}$$

Force

$$\sigma_\ell = \frac{-1.932\,V_o}{\lambda t^2} = -5{,}596 \text{ psi} \qquad \text{(D-9)}$$

$$\sigma_h = \frac{-2\,V_o\,\lambda\,R}{t} = -9{,}570 \text{ psi} \qquad \text{(D-10)}$$

(4) Stress Due to Discontinuity at Connector

As the worst case, the outer wrapper will be assumed to be built in. Thus, from Reference 12 Eqn 241:

$$M_o = P/2\,\beta^2 \qquad \text{(D-11)}$$

$$V_o = P/\beta \qquad \text{(D-12)}$$

$$\beta = \sqrt[4]{\frac{3\,(1-\nu^2)}{R^2\,t^2}} = 1.9393 \text{ in.}^{-1} \qquad \text{(D-13)}$$

At P = 70 psi,

M_o = 9.306 in-lb/in

V_o = -36.095 lb/in

And

$$\sigma_t = \frac{2\,\beta^2 R}{t}\left[\frac{V_o}{B} + M_o\right] \pm \nu\sigma_\ell \qquad \text{(D-14)}$$

$$\sigma_\ell = \pm\frac{6M_o}{t^2} \qquad \text{(D-15)}$$

Substituting known quantities:

	At OD	At ID
σ_ℓ =	-5,474 psi	5,474 psi
σ_t =	-4066 psi	-782 psi

(5) Stress Summary - Duct Outer Wrapper

Helix Area

	σ_ℓ	σ_h
Pressure	1,490 psi	2,980 psi
Shrink Fit	5,842 psi	11,684 psi

These stresses are interdependent and are not combined. As the pressure increases, the shrink decreases as do their stress components.

At End Cap (ID)

	σ_ℓ	σ_h
Primary Pressure	1,490 psi	2,980 psi
Secondary Moment	11,053 psi	6,087 psi
Secondary Force	-5,596 psi	-9,570 psi
Total (Primary and Secondary)	6,947 psi	-503 psi

At Connector

At OD

	σ_ℓ	σ_h
Primary Pressure	1,490 psi	2,980 psi
Secondary Bending	-5.474 psi	-4,066 psi
Total (Primary and Secondary)	-3,984 psi	-1,086 psi

At ID

	σ_ℓ	σ_h
Primary Pressure	1,490 psi	2,980 psi
Secondary Bending	5,474 psi	-782 psi
Total (Primary and Secondary	6,964 psi	2,198 psi

These stress values are within acceptable limits.

b. End Cap

(1) Primary Pressure Stress

The stress values for a circular plate, edges supported with a uniform load over the entire surface are given in Reference 11 page 194 Case 1:

$$\sigma_r = \frac{-3\ P\ r_a^2}{8\ m\ t^2} \left[(3m + 1)\ (1 - \frac{r^2}{r_o^2}) \right] \qquad \text{(D-16)}$$

and

$$\sigma_t = \frac{-3\ P\ r_o}{8\ m\ t^2} \left[(3m + 1) - (m + 3)\ \frac{r^2}{r_o^2} \right] \qquad \text{(D-17)}$$

At the plate center, the stresses are a maximum, r=o, (t=.625 in.)

$$\sigma_r = \sigma_t = -4{,}100 \text{ psi}$$

At the plate OD, $r=r_o$

$$\sigma_r = o$$

$$\sigma_t = -1{,}740 \text{ psi}$$

(2) Stress Due to Discontinuity at Outer Wrapper

From before, (eqn. D-3 and D-6) the reactions are:

$$M_o = 18.79 \text{ in-lb/in}$$

$$V_o = 57.29 \text{ lb/in}$$

The stresses resulting from these reactions are:

Moment

$$\sigma_r = \sigma_t = \frac{6M}{t^2} = -287 \text{ psi}$$

Force

$$\sigma_t = 0$$

$$\sigma_r = V_o / t = 92 \text{ psi}$$

(3) Stress Summary - Duct End Cap

At Center

	σ_r	σ_t
Primary Pressure	-4,100 psi	-4,100 psi
Secondary Moment	-287 psi	-287 psi
Secondary Force	92 psi	0 psi
Total (Primary and Secondary)	-4,295 psi	-4,387 psi

At OD

	σ_r	σ_t
Primary Pressure	0 psi	-1,740 psi
Secondary Moment	-287 psi	-287 psi
Secondary Force	92 psi	0 psi
Total (Primary and Secondary)	-195 psi	-2,027 psi

These stress values are within acceptable limits.

c. Intermediate Cylinder

(1) Primary Pressure Stress

$$\sigma_\ell = \frac{PR}{2t} = \frac{70 \times 3.20}{2 \times .08} \qquad \text{(D-18)}$$

$$\sigma = -1{,}400 \text{ psi}$$

$$\sigma_t = 2\,\sigma_\ell = -2{,}800 \text{ psi}$$

(2) Stress Due to Bending of Separators

From eqn. D-30 the moment caused by the bending of the separator is

$$M = 40.541 \text{ in-lb or } 2.016 \text{ in-lb/in}$$

The stress in the cylinder due to this moment is, from Reference 11:

$$\sigma_\ell = \frac{\pm\, 6M_o}{t^2} \qquad \text{(D-19)}$$

$$\sigma_\ell = \pm\, 1{,}890 \text{ psi}$$

$$\sigma_h = \frac{\pm 2M_o \lambda^2 R}{t} \qquad \text{(D-20)}$$

$$\lambda^2 = \sqrt{\frac{3(1-\nu^2)}{R^2 T^2}} = 6.537 \text{ in.}^{-2} \qquad \text{(D-21)}$$

$$\sigma_h = 1041 \text{ psi}$$

(3) End Reaction

For a cylinder with fixed ends, external pressure, Reference 11 gives the reactions as: see eqn. (D-11 and D-12)

$$M_o = -P/2\beta^2 = -.819 \text{ in-lb/in} \qquad \text{(D-22)}$$

$$V_o = P/\beta = 10.708 \text{ lb/in} \qquad \text{(D-23)}$$

From eqns. D-14 and D-15, the stresses due to these reactions are:

	At OD	At ID
σ_ℓ	768 psi	-768 psi
σ_t	2,981 psi	2,521 psi

(4) Stress Summary - Duct Intermediate Cylinder

Under Helix

	σ_ℓ	σ_h
Pressure	-1,400 psi	-2,800 psi
Moment	±1,890 psi	±1,041 psi
Total	-3,290 psi	-3,841 psi

At Ends - ID

	$\sigma\ell$	σ_h
Primary Pressure	-1,400 psi	-2,800 psi
Secondary Bending	-768 psi	2,521 psi
Total	-2,168 psi	-279 psi

At Ends - OD

	$\sigma\ell$	σ_h
Primary Pressure	-1,400 psi	-2,800 psi
Secondary Bending	+768 psi	2,981 psi
Total	-632 psi	181 psi

These stress values are within acceptable limits.

d. Inner Cylinder - Duct

(1) Primary Pressure Stress

$$\sigma_\ell = \frac{PR}{2t} = \frac{70 \times 1.675}{2 \times .05} = 1{,}173 \text{ psi} \quad \text{(D-24)}$$

$$\sigma_h = 2\,\sigma_\ell = 2{,}346 \text{ psi} \quad \text{(D-25)}$$

(2) End Reaction

$$\beta = \sqrt[4]{\frac{3(1-\nu^2)}{R^2 t^2}} = 4.4417 \text{ in.}^{-1} \quad \text{(D-26)}$$

$$M_o = P/2\beta^2 = 1.774 \text{ in-lb/in} \quad \text{(D-27)}$$

$$V_o = -P/\beta = -15.759 \text{ lb/in} \quad \text{(D-28)}$$

The stresses due to these reactions are:

	At OD	At ID
σ_ℓ	-4,258 psi	4258 psi
σ_h	-3,622 psi	-7,068 psi

(3) Stress Summary - Duct Inner Cylinder

At OD

	σ_ℓ	σ_h
Primary Pressure	1,173 psi	2,346 psi
Secondary Bending	-4,258 psi	-3,622 psi
Total	-3,085 psi	-1,276 psi

At ID

	σ_ℓ	σ_h
Primary Pressure	1,173 psi	2,346 psi
Secondary Bending	4,258 psi	-1,068 psi
Total	5,431 psi	1,278 psi

These stress values are within acceptable limits.

e. Helix

As a worst case, it will be assumed that the thread lead is constant at 1.28 inch.

The differential pressure across each separator is:

$$\Delta P = \frac{P \times \text{lead}}{\text{Length}} = \frac{70 \times 1.28}{18} \qquad \text{(D-29)}$$

$$\Delta P = 2.844 \text{ psi}$$

The separator is essentially a cantilever beam. The pressure causes a maximum moment of:

$$M = \Delta P \pi \left(\frac{d_o + d_i}{2}\right)\left(\frac{d_o - d_i}{2}\right)\left(\frac{d_o - d_i}{4}\right) \qquad \text{(D-30)}$$

$$M = 2.844\pi\,(7.5)(1.1)(.55) = 40.541 \text{ in-lb}$$

$$c = t/2 = .06/2 = .03 \text{ in} \qquad \text{(D-31)}$$

$$I = bd^3/12 = 1/12\left[\pi\left(\frac{d_o + D_i}{2}\right) t^3\right] = .4241 \times 10^{-3} \text{in}^4 \qquad \text{(D-32)}$$

$$\sigma = \frac{Mc}{I} = 2{,}868 \text{ psi} \qquad \text{(D-33)}$$

This stress is within acceptable limits

f. Inlet/Outlet Pipes

(1) Primary Pressure

$$\sigma_\ell = \frac{PR}{2t} = \frac{70 \times 2.190}{2 \times .120} = 639 \text{ psi} \qquad \text{(D-34)}$$

$$\sigma_h = 2\sigma_\ell = 1278 \text{ psi} \qquad \text{(D-35)}$$

(2) End Reaction (Built-In)

$$\beta = \sqrt[4]{\frac{3(1-\nu^2)}{R^2 t^2}} = 2.5075 \qquad \text{(D-36)}$$

$$M_o = P/2\beta^2 = 5.567 \text{ in-lb/in} \qquad \text{(D-37)}$$

$$r_o = -P/\beta = -27.916 \text{ lb/in} \qquad \text{(D-38)}$$

The stresses due to these reactions are:

	At OD	At ID
σ_ℓ	-2,320 psi	2,320 psi
σ_h	-1,973 psi	-581 psi

(3) Stress Summary - Duct Inlet/Outlet Pipes

At OD

	σ_ℓ	σ_h
Primary Pressure	639 psi	1,278 psi
Secondary Bending	-2,320 psi	-1,973 psi
Total	-1,681 psi	-695 psi

At ID

	σ_ℓ	σ_h
Primary Pressure	639 psi	1,278 psi
Secondary Bending	2,320 psi	-581 psi
Total	2,959 psi	697 psi

These stress values are within acceptable limits.

g. Center Core Exchanger Wrapper

(1) Primary Pressure (outer wrapper)

$$\sigma_\ell = \frac{PR}{2t} = \frac{25 \times (2.24)}{2\ (.060)} = 467 \text{ psi} \qquad \text{(D-39)}$$

$$\sigma_h = 2\sigma_\ell = 934 \text{ psi} \qquad \text{(D-40)}$$

(2) End Reactions

As a worst case this heat exchanger is assumed to be built in. (See eqns. D-11, D-12, and D-13).

β = 3.506 lb/in

M_o = 1.017 in-lb/in

V_o = -7.131 lb/in

From eqns. D-14 and D-15 the resulting stresses are:

	At OD	At ID
σ_ℓ	-1,695 psi	1,695 psi
σ_h	-1,441 psi	-425 psi

(3) Stress Summary - Center Core Heat Exchanger Outer Wrapper

At ID

	σ_ℓ	σ_h
Primary	467 psi	934 psi
Secondary Bearing	1,695 psi	-425 psi
Total	2,162 psi	509 psi

At OD

	σ_ℓ	σ_h
Primary	467 psi	934 psi
Secondary Bending	-1,695 psi	-1,441 psi
Total	-1,228 psi	-507 psi

These stresses are within acceptable limits.

(4) Inlet/Outlet Pipes and Inner Wrapper

Since the radii of the pipes and the inner wrapper are less than that of the outer wrapper the stresses in these parts will be less than those recorded in (3) above.

h. End Shields

In the duct there are three circular end shields with holes at their centers which are supported at the outside and inside edges. They are located between the outer wrapper and the intermediate cylinder, the intermediate cylinder and inner cylinder, and at the ends of the small heat exchanger. From Reference 11, page 198 cases 13 and 14, the primary stresses in these end shields are significantly less than the primary stresses in the adjoining cylinders. It is also seen that since these end shields are materially thicker than the adjoining cylinders

that the secondary stresses are also less than those in the cylinder; hence these end shields are acceptable.

2. Frame and Stator Heat Exchanger

The maximum stress values used in this section are, based on 900°F:

Material	σ_{max}	σ_y (.2%)	Reference
Inconel	14,900 psi	19,200 psi	3 and 6
Hastelloy B	16,600 psi	39,300 psi	4 and 5

a. Internal Pressure

The pump frame will be filled with inert gas to 6-9 psia at room temperature. During operation, this gas will become heated to a maximum of 1050°F. This will result in a corresponding pressure of:

$$P_o = P_r \frac{T_o}{T_R} = 9 \frac{(1050 + 460)}{70 + 460)} \qquad \text{(D-41)}$$

$$P_o = 25.6 \text{ psia}$$

Since this pump is designed to operate in a vacuum, the design pressure will be:

$$P = 30 \text{ psi}$$

b. Outer Shell - Connection End - Inconel

$$\sigma_\ell = \frac{PR}{2t} = \frac{30 \times 7.8625}{2 \times .125} = 944 \text{ psi} \qquad \text{(D-42)}$$

$$\sigma_h = 2\sigma_\ell = 1887 \text{ psi} \qquad \text{(D-43)}$$

(2) Reaction at End Shield

$$\lambda = \sqrt[4]{\frac{3(1-\nu^2)}{R^2 t^2}} = 1.2966 \text{ in.}^{-1} \qquad \text{(D-44)}$$

$$D = \frac{Et^3}{12(1-\nu^2)} \qquad \text{(D-45)}$$

$$D_1 = 184{,}676 \text{ in-lb}; \quad D_2 = 4{,}293 \text{ in-lb}$$

$$M_o = \frac{\left[\frac{Pr^3 \lambda^2 D_2}{4D_1(1+\nu)} + \frac{2 P R^2 \lambda^3 Et_1 D_2}{Et_2(1-1/2\nu)\left[Et_1 + 2RD_2\lambda^3 (1-\nu)\right]}\right]}{\left[2\lambda + \frac{2 R \lambda^2 D_2}{D_1 (1+\nu)} - \frac{\lambda Et_1}{Et_1 + 2 D_2 \lambda^3 R (1-\nu)}\right]} \quad \text{(D-46)}$$

Substituting known values

$M_o = 69.06$ in-lb/in

$$V_o = M_o \left[2\nu + \frac{2R \lambda^2 D_2}{D_1 (1+\nu)}\right] - \left[\frac{PR^3 \lambda^2 D_2}{4 D_1 (1+\nu)}\right] \quad \text{(D-47)}$$

$V_o = 102.15$ lb/in

The stresses at the ID due to these reactions are:

Moment

$$\sigma_\ell = \frac{6 M_o}{t^2} = 26{,}520 \text{ psi} \quad \text{(D-48)}$$

$$\sigma_h = \frac{2 M_o \lambda^2 R}{t} = 14{,}606 \text{ psi} \quad \text{(D-49)}$$

Force

$$\sigma_\ell = \frac{-1.932 V_o}{\lambda t^2} = -9{,}741 \text{ psi} \quad \text{(D-50)}$$

$$\sigma_h = \frac{-2 V_o \lambda R}{t} = -16{,}662 \text{ psi} \quad \text{(D-51)}$$

(3) Reaction at Hastelloy B Junction

A thermal stress is generated at the junction of the Inconel and Hastelloy B due to the different coefficients of thermal expansion. This differential expansion is:

$$\Delta\delta = \Delta T R (\alpha_I - \alpha_H) \quad \text{(D-52)}$$

$\Delta\delta = (830)(7.8625)(8.0 \times 6.6)\ 10^{-6}$

$\Delta\delta = 9.136 \times 10^{-3}$ inch

Each of the two cylinders will be deflected a portion of this expansion, in proportion to their moduli of elasticity. Thus:

$$\delta_I = \left(\frac{24}{24 + 24.8}\right) \quad 9.136 \times 10^{-3} = 4.493 \times 10^{-3} \text{ in.}$$

$$\delta_H = 4.643 \times 10^{-3} \text{ in.}$$

From Reference 12, equation 241,

$$M_o = 2 \lambda D_2 \delta_H = 67.019 \text{ in-lb/in} \qquad \text{(D-53)}$$

$$V_o = 2 \lambda M_o = 179.09 \text{ lb/in} \qquad \text{(D-54)}$$

The resultant stresses at the ID are:

Moment

$$\sigma_\ell = 6 M_o / t^2 = -25,742 \text{ psi} \qquad \text{(D-55)}$$

$$\sigma_h = 2 M_o \lambda^2 R/t = 14,174 \text{ psi} \qquad \text{(D-56)}$$

Force

$$\sigma_\ell = \frac{1.932 V_o}{\lambda t^2} = 17,078 \text{ psi} \qquad \text{(D-57)}$$

$$\sigma_h = 2 V_o \lambda R/t = 29,200 \text{ psi} \qquad \text{(D-58)}$$

(4) Stress Summary - Outer Shell - Connection End - Inconel

At End Shield (at the ID)

	σ_ℓ	σ_h
Primary Pressure	944 psi	1,887 psi
Secondary Moment	26,520 psi	14,606 psi
Secondary Force	-9,741 psi	-16,662 psi
Total	17,723 psi	-169 psi

At Hastelloy B (at the ID)

	σ_ℓ	σ_h
Primary Pressure	944 psi	1,887 psi
Thermal Moment	25,742 psi	14,174 psi
Thermal Force	17,078 psi	29,200 psi
Total	43,764 psi	45,261 psi

The stress values are within acceptable limits. The high stress at the Hastelloy B junction is mainly a thermal stress.

c. Outer Shell - Hastelloy B

(1) Primary Pressure Stress

From Equations D-42 and D-43:

σ_ℓ = 944 psi

σ_h = 1887 psi

(2) Reaction at Inconel Junction

The moment and force will be equal and opposite to those in the inconel shell. Thus,

M_o = 67.019 in-lb/in

V_o = 179.09 lb/in

Since the material thicknesses and Poisson's ratios are the same, the stresses at the ID will be:

Moment

σ_ℓ = 25,742 psi

σ_h = 17,078 psi

Force

σ_ℓ = -17,078 psi

σ_h = -29,200 psi

(3) Reaction at Heat Exchanger

For conservatism, the heat exchanger will be treated as fixed.

Thus,

$$\beta = \sqrt[4]{\frac{3\,(1-\nu^2)}{R^2\,t^2}} = 1.2966 \text{ in.}^{-1} \qquad \text{(D-59)}$$

$$M_o = P/2\,\beta^2 = 8.922 \text{ in-lb/in} \qquad \text{(D-60)}$$

$$V_o = -P/\beta = -23.137 \text{ lb/in} \qquad \text{(D-61)}$$

The resultant stresses are:

$$\sigma_h = \frac{6\,(1-\nu^2)}{\beta^2\,t^2\,R}\left[\frac{V_o + M_o}{P}\right] \pm \nu\sigma_\ell \qquad \text{(D-62)}$$

$$\sigma_\ell = \pm\, 6\, M_o\, /t^2 \qquad \text{(D-63)}$$

Substituting known quantities:

	At OD	At ID
σ_ℓ	-3,426 psi	3,426 psi
σ_h	-2,915 psi	-859 psi

(4) Stress Summary - Outer Shell - Hastelloy B

At Inconel

	σ_ℓ	σ_h
Primary Pressure	944 psi	1,887 psi
Thermal Moment	25,742 psi	14,174 psi
Thermal Force	-17,078 psi	-29,200 psi
Total	9,608 psi	-13,139 psi

At Heat Exchanger

	σ_ℓ	σ_h
Primary Pressure	944 psi	1,887 psi
Secondary Bending	3,426 psi	-859 psi
Total - ID	4,370 psi	1,028 psi

These stress values are within acceptable limits

d. End Shield - Connection End - Inconel

(1) Primary Pressure Stress

The stress values for a circular plate, edges supported, with a uniform load over the entire surface are given in Reference 11 page 194 Case 1.

$$\sigma_r = \frac{-3Pr_o^2}{8\,m\,t^2}\left[(3\,m+1)\left(1-\frac{r^2}{r_o^2}\right)\right] \qquad \text{(D-64)}$$

and

$$\sigma_t = \frac{-3PR_o^2}{8\,m\,t^2}\left[(3\,m+1)-(m+3)\frac{r^2}{r_o^2}\right] \qquad \text{(D-65)}$$

At the plate center, the stresses are a maximum, r=o (t=.438 in.)

$\sigma_r = \sigma_t = -11{,}800$ psi

At the plate OD, $r = r_o$

$\sigma_r = 0$

$\sigma_t = -5{,}006$ psi

(2) End Reaction

From before:

$M_o = 69.06$ in-lb/in

$V_o = 102.13$ lb/in

The resultant stresses are:

Moment

$$\sigma_r = \sigma_t = 6\,M/t^2 = -2{,}165 \text{ psi}$$

Force

$$\sigma_t = 0$$

$$\sigma_r = V_o/t = 233 \text{ psi}$$

(3) Stress Summary - End Shield - Connection End - Inconel

At ID

	σ_r	σ_t
Primary Pressure	-11,800 psi	-11,800 psi
Secondary Moment	-2,165 psi	-2,165 psi
Secondary Force	233 psi	0 psi
Total	-13,732 psi	-13,965 psi

At OD

	σ_r	σ_t
Primary Pressure	0 psi	-5,006 psi
Secondary Moment	-2,165 psi	-2,165 psi
Secondary Force	233 psi	0 psi
Total	-1,932 psi	-7,171 psi

These stress values are within acceptable limits.

e. Outer Shell - Opposite Connection End

(1) Primary Pressure Stress

$$\sigma_\ell = PR/2t = \frac{30 \times 7.8625}{2 \times .125} = 944 \text{ psi}$$

$$\sigma_h = 2\sigma_\ell = 1{,}888 \text{ psi}$$

(2) Reaction at End Shield

$$\lambda = \sqrt[4]{\frac{3\,(1-\nu^2)}{R^2\,t^2}} = 1.2966 \text{ in.}^{-1}$$

$$D = \frac{Et^3}{12(1-\nu^2)}$$

D_1 = 274,725 in-lb (t = .500 in.)

D_2 = 4293 in-lb (t = .125 in.)

Using the same type analysis as before: (see Equations D-46 to D-49)

M_o = 53.62 in-lb/in

V_o = -82.43 lb/in

The resultant stresses at the ID are:

	Moment	Force
σ_ℓ =	20,590 psi	-7,861 psi
σ_h =	11,340 psi	-13,446 psi

(3) Reaction at Hastelloy B Junction

These stresses will be identical with those at the connection end.

(4) Stress Summary - Outer Shell - Opposite Connection End

	σ_ℓ	σ_h
Primary Pressure	944 psi	1,888 psi
Secondary Moment	20,590 psi	11,340 psi
Secondary Force	-7,861 psi	-13,446 psi
Total	-13,673 psi	-218 psi

These stress values are within acceptable limits.

f. End Shield - Opposite Connection End

(1) Primary Pressure Stress

From Reference 11, page 198, Case 13, the maximum stress is:

$$\sigma_{max} = \sigma_t = \frac{-3P}{4\,m\,t^2(r_o^2 - r_i^2)} \left[r_o^4 (3m+1) + r_i^4 (m-1) - 4m r_o^2 r_i^2 - 4(m+1) r_o^2 r_i^2 \ln(r_o / r_i) \right]$$

Substituting known values:

$$\sigma_{max} = -9{,}196 \text{ psi}$$

(2) End Reactions

From e(2) these reactions are:

$$M_o = 53.62 \text{ in-lb/in}$$

$$V_o = -82.43 \text{ lb/in.}$$

From Reference 11 page 201, Case 25 for moment

$$\sigma_r = \frac{6 M_o r_o^2}{t^2 (r_o^2 - r_i^2)} \left[1 - \frac{r_i^2}{r^2} \right] \qquad \text{(D-71)}$$

$$\sigma_t = \frac{6 M_o r_o^2}{t^2 (r_o^2 - r_i^2)} \left[1 + \frac{r_i^2}{r^2} \right] \qquad \text{(D-72)}$$

Substituting known quantities:

At $r = r_o$

$$\sigma_r = 1{,}287 \text{ psi}$$

$$\sigma_t = 2{,}595 \text{ psi}$$

At $r = r_i$

$$\sigma_r = 0$$

$$\sigma_t = 3{,}881 \text{ psi}$$

Force

$\sigma_r = -V_o / t = 165$ psi

$\sigma_t = 0$

(3) Secondary Pressure Stress

From Reference 11, page 198, Case 14, the maximum stress, for a circular plate with a hole and uniformly loading at the inside radius, is located at the inside radius and is

$\sigma_{max} = \sigma_t = -10,745$ psi

where the uniform load is 1900 lb.

(4) Stress Summary - End Shield - Opposite Connection End

At $r = r_o$

	σ_r	σ_t
Primary Pressure	-9,196 psi	-9,196 psi
Secondary Moment	1,287 psi	2,595 psi
Secondary Force	165 psi	0 psi
Total	-7,744 psi	-6,601 psi

At $r = r_i$

	σ_r	σ_t
Primary Pressure	-9,196 psi	-9,196 psi
Secondary Pressure	-10,280 psi	-10,280 psi
Secondary Moment	0 psi	3,881 psi
Secondary Force	165 psi	0 psi
Total	-19,311 psi	-15,595 psi

These stresses are within acceptable limits.

g. Stator Heat Exchanger

(1) Differential Thermal Expansion Between Heat Exchanger and Stator Punchings

Assuming a ΔT of 650°F, the radial differential expansion is:

$$\Delta\delta = R\,\Delta T\,(\alpha_H - \sigma_p) \qquad \text{(D-73)}$$

$$\Delta\delta = 7.8625 \times 650\,(6.5 - 5.95) \times 10^{-6} = 2.8 \times 10^{-3} \text{ in.}$$

Stress Due to Differential Thermal Expansion

These stresses must be evaluated under two conditions: non-operating or room temperature and operating. These two conditions impose differing methods of loading on the heat exchanger.

At room temperature, the main loading is due to the interference fit. In addition, the pressure is external at about 7-9 psi. Since this pressure is opposite to that caused by the interference fit, it will be neglected.

Assume radial shrink fit of 5×10^{-3} inch

$$\sigma = \frac{R}{E}\,(2-\nu)\,\sigma_\ell \qquad \text{(D-74)}$$

Solving for σ_ℓ

$\sigma_\ell = 8.978$ psi

$\sigma_h = 17{,}956$ psi

Under operating conditions, the stress due to the interference fit will be greatly reduced due to the greater expansion of the heat exchanger.

(3) Summary - Heat Exchanger

Some yielding of the heat exchanger may occur during assembly; however, under these circumstances, the stresses would be relieved. Any sustained stress or yield would not affect the operation of the pump. Thus, these stresses are acceptable.

h. Stator Heat Exchanger Wrapper

(1) Interference Fit

Assume 2×10^{-3} inch interference fit:

$$\sigma_\ell = E\delta/R(2-\nu) = 3{,}653 \text{ psi} \quad \text{(D-75)}$$

$$\sigma_h = 7{,}306 \text{ psi}$$

(2) Internal Pressure (design pressure = 25 psi)

$$\sigma_\ell = PR/2t = 799 \text{ psi} \quad \text{(D-76)}$$

$$\sigma_h = 2\sigma_\ell = 1{,}598 \text{ psi} \quad \text{(D-77)}$$

(3) End Reactions

Using the method of Reference 12 (see equations 59, 60 and 61):

$$\beta = 1.286 \text{ in.}^{-1}$$

$$M_o = 7.558 \text{ in-lb/in}$$

$$V_o = -19.440 \text{ lb/in}$$

The resulting stresses are:

	At OD	At ID
σ_ℓ	-2,902 psi	2,902 psi
σ_h	-2,443 psi	-701 psi

(4) Stress Summary - Heat Exchanger Wrapper

At ID	σ_ℓ	σ_h
Primary Pressure	799 psi	1,598 psi
Secondary Bending	2,902 psi	-701 psi
Total	3,701 psi	897 psi

At OD	σ_ℓ	σ_h
Primary Pressure	799 psi	1,598 psi
Secondary Bending	-2,902 psi	-2,443 psi
Total	-2,103 psi	-845 psi

These stress values are within acceptable limits.

i. Stator Can

(1) Geometry

The stator can is a thin short tube exposed to lateral external pressure and to axial external pressure at one end. The ends of the tube are welded to relatively thick circular members; the tube is continuously restrained at its OD and ID by the stator can support structure and the duct/insulation structure respectively.

Fig. D1

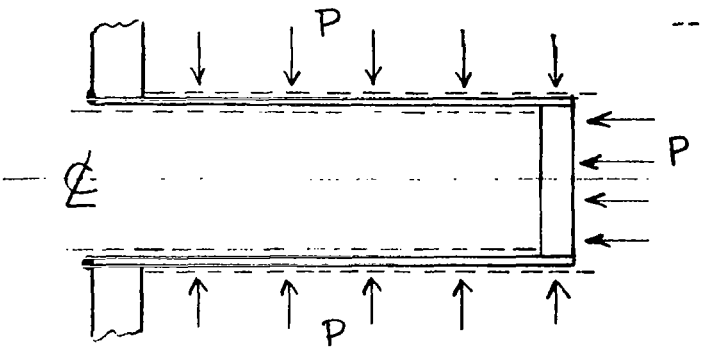

(2) Analytical Analysis

The precise geometry described above (Fig. D1), is not specifically analyzed in literature; however, a realistic application of previous theory will be presented.

Theoretical solution to the question of the collapse of thin short tubes was given by Von Mises (Reference 11, page 318, equation 32) for external pressure in lateral and axial directions, and with the restraint that the ends of the tube be held circular. This solution is:

$$P = \frac{Et}{r} (A + L) \qquad \text{(D-78)}$$

where:

$$A = \frac{1}{\left[1 + \frac{1}{2}\left(\frac{\pi r}{n\ell}\right)^2\right] n^2 \left[1 + \left(\frac{n\ell}{\pi r}\right)^2\right]^2}$$

$$L = \frac{\left[1 + \left(\frac{\pi r}{n\ell}\right)^2\right]^2}{\left[1 + \frac{1}{2}\left(\frac{\pi r}{n\ell}\right)^2\right]} \left[\frac{n^2 t^2}{12 r^2 (1-\nu)^2}\right]$$

Note that all geometric values are known except for n, the number of lobes that the tube will develop in buckling. Since the can is restrained at its OD and ID, it cannot buckle until the circumferential length of the can has been accommodated. Each confrontation of the can with the support structures at the OD and ID will compel the can to develop more lobes. The sums of the radial gaps between the can and the two support structures is 0.049-0.083 in.

Based on collapse data and previous analytical study, it was assumed that the can lobes will follow the form of a sine wave. As an approximation a triangular configuration was used, see Fig. D2 below.

Figure D2

Mean dia. of can = 9.156 in.
Min. OD of duct/insulation = 9.012 in.

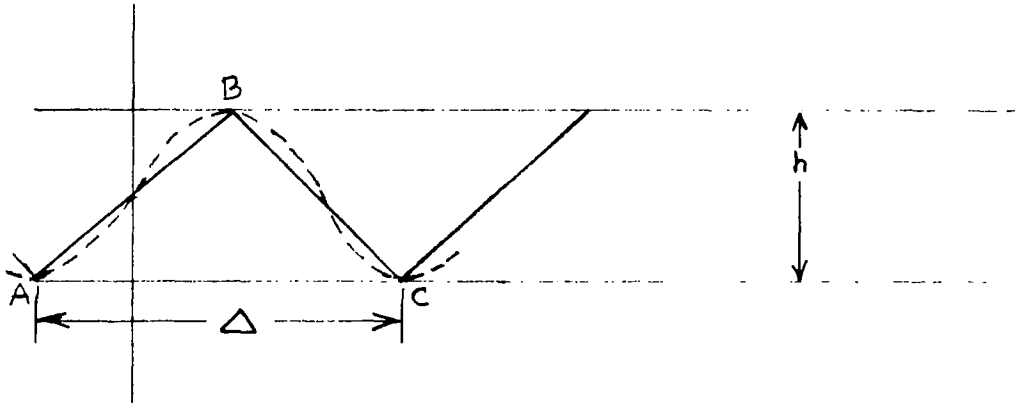

Let AB = BC

$$\left(\frac{C}{2}\right)^2 = h^2 t \left(\frac{\Delta}{2}\right)^2 \qquad \text{(D-79)}$$

$$n\Delta = \pi(9.012) \qquad \text{(D-80)}$$

$$nC = \pi(9.156) \qquad \text{(D-81)}$$

The solution of equations D-79, D-80 and D-81 is:

$n = 30.662$

$\Delta = 0.9244$

$C = 0.9392$

It can be shown that a sine wave for this basic dimension will differ less than 1% from the straight line triangular shape. Therefore n was conservatively taken as 30.

Equation D-78 yields, for the minimum can thickness of 0.025 in., a buckling pressure of:

$P = 343$ psi.

In equation D-78, expression A represents the contribution of the axial pressure and expression L represents the contribution of the lateral pressure. It should be noted that the axial pressure increases the buckling pressure; for this example the effect of expression A is less than 2%. It is seen that the buckling pressure is more than 10 times the design can pressure of 30 psi.

(3) Experimental Data

Although experimental data for the precise geometry in Figure D1 is not available, useful data that supports the above analytical evaluation is available.

Stator cans with lateral external pressure, restricted at the OD and at the ends but without axial loading and without any restriction at the ID have been tested. The following observations were noted:

(a) the cans tended to form a 20-24 lobal system.

(b) as the external pressure was increased collapse results with the can in a 4 lobe system due to a lack of restraints at the can ID.

(c) experimental values for K of 1.8 in equation D-82 was determined for the geometry described above.

$$P = K \frac{t^3}{d} \qquad \text{(D-82)}$$

where t is in mils (25)

d is in inches (9.158)

The resulting collapse pressure for a can without any restraint at the ID and without axial loading is

$P = 36.6$ psi.

Obviously, had the ID been restricted to a maximum clearance of .083 in. instead of zero support the can would not have settled into a 4 lobe system and the buckling pressure would have been significantly higher.

(4) Conclusion

Analytical evaluation and experimental observations indicate that the buckling strength of the stator can of this design is adequate for an external design pressure of 30 psi.

j. Stator Can Welds

Of the two can welds, the weld-opposite the connector end is more highly loaded. It is assumed that the can is built-in the can support structure at the weld. Since the weld is thicker than the can, the highest stresses will be in the can itself.

From Reference 11, page 271, Case 9 and Figure D3, below.

$$M = .304\ Pr\ t \qquad \text{(D-83)}$$

$$V = .78\ P\ rt \qquad \text{(D-84)}$$

$$\lambda = \sqrt[4]{\frac{3\ (1-\nu)}{r^2\ t^2}} \qquad \text{(D-85)}$$

$$F = P\ \pi\ (2r + t) \qquad \text{(D-86)}$$

$$M = 1.04\ \text{in-lb/in}$$

$$V = 7.92\ \text{in-lb}$$

$$\lambda = 3.80\ \text{in.}^{-1}$$

$$F = 1986\ \text{lb}$$

From Figure D3, the stresses at the OD are:

$$\sigma_\ell = \frac{6M}{t^2} + \frac{F}{2\pi\ rt}$$

$$\sigma_h = \frac{-2M}{t}\ \lambda^2\ r + \frac{2V}{t}\ \lambda r + \nu\ \sigma_\ell$$

$$\sigma_r = -P$$

Figure D3

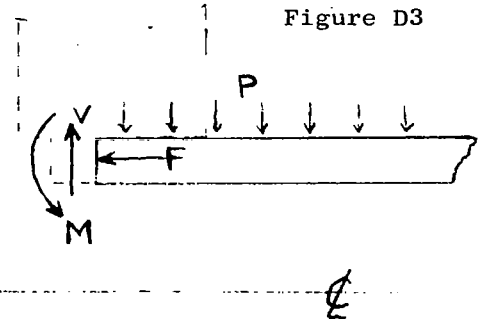

σ_ℓ = 12,747 psi

σ_h = 9,348 psi

σ_r = -30 psi

All stress values are within acceptable limits.

k. Stator Can End Plate

Considering this end plate as a uniformly loaded circular plate simply supported at its outer edge, the maximum stresses per equation D-16 and D-17 are:

At the center of the plate (r = 0)

$\sigma_{max} = \sigma_r - \sigma_t$ = 3150 psi

At the plate OD ($r = r_o$)

σ_r = 0

σ_t = 1340 psi

The rotation at the outer edge per Reference 11, page 194, Case 1

$$\theta = \frac{3W\,(m-1)\,r_o}{2\pi\,E\,m\,t^3} \qquad \text{(D-87)}$$

θ = .007 radians

The deflection due to this rotation at $r = r_o$ is

$\delta = \theta t$ = .0035 in.

These values are within acceptable limits.

E. DESIGN DATA AND PHYSICAL PROPERTIES

Summary

(References 1-7, 14, 16, 17 & 18)

1. Lithium Properties (primary fluid at 2100°F)

a.	electrical resistivity	19.9 μΩ in.
b.	density	26.1 lb/ft^3
c.	specific heat	0.985 Btu/lb °F
d.	thermal conductivity	0.989 W/°F in
e.	viscosity	0.64 lb/hr ft

2. Duct Properties - T-111 alloy at 2100°F

a.	electrical resistivity	25.2 μΩ in
b.	density	0.6 lb/in^3
c.	thermal conductivity	0.767 W/°F in
d.	thermal coefficient of expansion (from room temperature)	4.2×10^{-6} in/in. °F

3. Winding Properties

a.	effective electrical resistivity of conductor at 1050°F (Ni-clad Ag)	2.32 μΩ in.
b.	density of conductor	0.367 $lb/in.^3$
c.	effective thermal conductivity of conductor	4.53 W/°F in.
d.	effective thermal resistivity of electrical slot insulation (ceramic and gas)	108 °F in/W

4. Magnetic Material Properties (Hiperco 27)

a.	density	0.285 $lb/in.^3$
b.	thermal resistivity	0.486 °F in/W
d.	approx. core loss factor at 60 Hz; 0.025 in. thick lamination	4 W/lb.

d.	thermal coefficient of expansion (77°-900°F)	5.96×10^{-6} in/in °F

5. Other Design Data and Properties

a.	density of Inconel	0.31 $lb/in.^3$
b.	density of Hastelloy B	0.33 $lb/in.^3$
c.	electrical resistivity of Inconel can at 1000°F	41 μΩ in.
d.	estimated effective thermal resistivity of foil thermal insulation in vacuum (used primarily as radiation shields)	630 °F in./W
e.	thermal coefficient of expansion of Hastelloy B	6.4×10^{-6} in/in °F
f.	thermal coefficient of expansion of Inconel	7.5×10^{-6} in/in °F

6. NaK Properties (coolant)

a.	density at 800°F	48.2 lb/ft^3
b.	specific heat at 800°F	0.208 Btu/lb °F
c.	viscosity at 800°F	0.473 lb/hr ft

VII. REFERENCES

1. Verkamp, J.P. and Rhudy, R.G., "Electromagnetic Alkali Metal Pump Research Program," Report NASA CR-380, General Electric Company, February 1966.

2. Diedrich, G.E. and Gahan, J.W., "Design of Two Electromagnetic Pumps," Report NASA CR-911, General Electric Company, November 1967.

3. Pendleton, W.W., "Radiation-Resistant Magnet Wire for Use in Air and Vacuum at 850°C," Technical Documentary Report ASD-TDR-63-164, Anaconda Wire and Cable Company, July 1963.

4. Kueser, P.E., et al., "Development and Evaluation of Magnetic and Electrical Materials Capable of Operating in the 800°F to 1600°F Temperature Range," Report NASA CR-54354, First Quarterly Report, Westinghouse Electric Corporation, March 1965.

5. Kueser, P.E., et al., "Development and Evaluation of Magnetic and Electrical Materials Capable of Operating in the 800°F to 1600°F Temperature Range," Second Quarterly Report, June 1965.

6. Kueser, P.E. et al., "Magnetic Materials Topical Report," Report NASA CR-54091, Westinghouse Electric Corporation, September 1964.

7. Kueser, P.E., et al., "Electrical Conductors and Electrical Insulating Materials Topical Report," Report NASA CR-54092, Westinghouse Electric Corporation, October 1964.

8. Blake, L.R., "Conduction and Induction Pumps for Liquid Metals," Proc. IEE, Part A, Vol. 104, No. 13, February 1957.

9. Watt, D.A., "The Design of Electromagnetic Pumps for Liquid Metals," Paper No. 2763, IEE, December 1958.

10. Alger. P.S., "The Nature of Polyphase Induction Machines," John Wiley & Sons, Inc., 1951.

11. Roark, R.J., "Formulas for Stress and Strain," McGraw-Hill Book Company, Inc. 1943.

12. Timoshenko, S., "Theory of Plates and Shells," McGraw-Hill Book Company, Inc., 1959.

13. ASME Boiler and Pressure Vessel Code, Section VIII, "Unfired Pressure Vessels," 1965 Edition.

14. "Hastelloy Alloy B," Haynes Stellite Company, 1962.

15. ASME Boiler and Pressure Vessel Code, Code Case 11348.

REFERENCES (Continued)

16. International Nickel Company, "Engineering Properties of Inconel," 1963.

17. Lyon, R.N., Ed., "Liquid Metals Handbook," Revised, Second Edition, U.S. Government Printing Office, Washington, D.C.

18. Jackson, C.B., Ed., "Liquid Metals Handbook-Sodium (NaK) Supplement," Third Edition, U.S. Government Printing Office, Washington, D.C.

19. Watt, D.A., "Single Phase Annular Induction Pump for Liquid Metals," A.E.R.E. ED/R 1844, Atomic Energy Research Establishment, Great Britain, March, 1953.

20. Schwirian, R.E., "Single Phase Induction Electromagnetic Pump," NASA TN D-3950, Lewis Research Center, National Aeronautics & Space Administration, May, 1967.

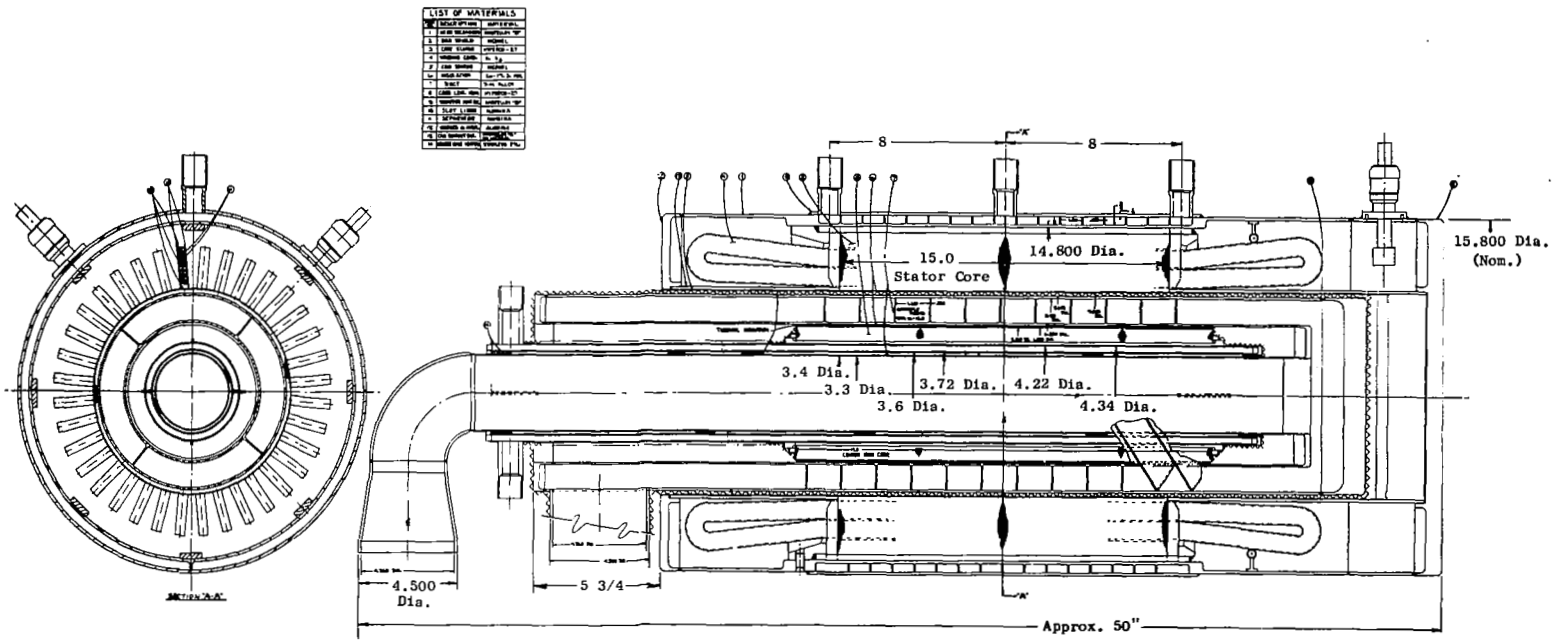

Figure 1. Helical Induction EM Pump with Center Return Flow - 25 Hz.
(Preliminary Design)

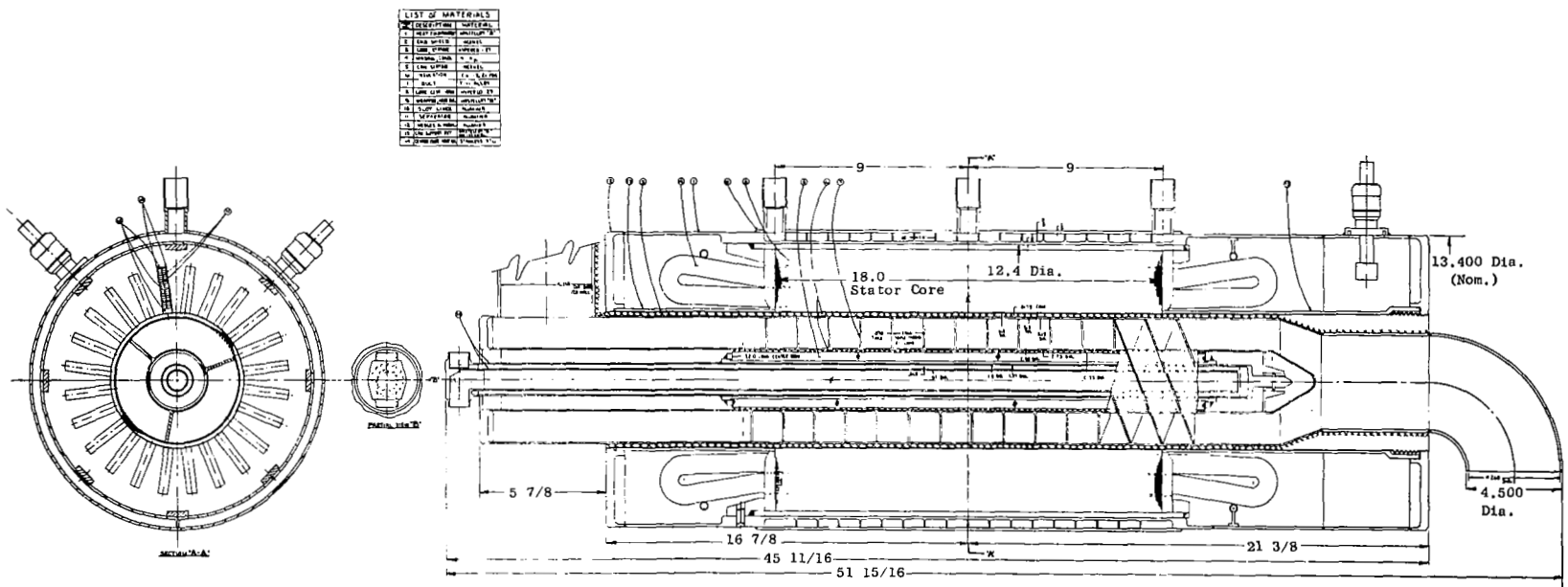

Figure 2. Helical Induction EM Pump - 60 Hz. (Preliminary Design)

NOTE: NaK Coolant Inlet Temperature, 800°F. Design Point Lithium Flow, 30 lb/sec, Lithium Inlet Temperature, 2100°F - Lithium Δp = 20 psi

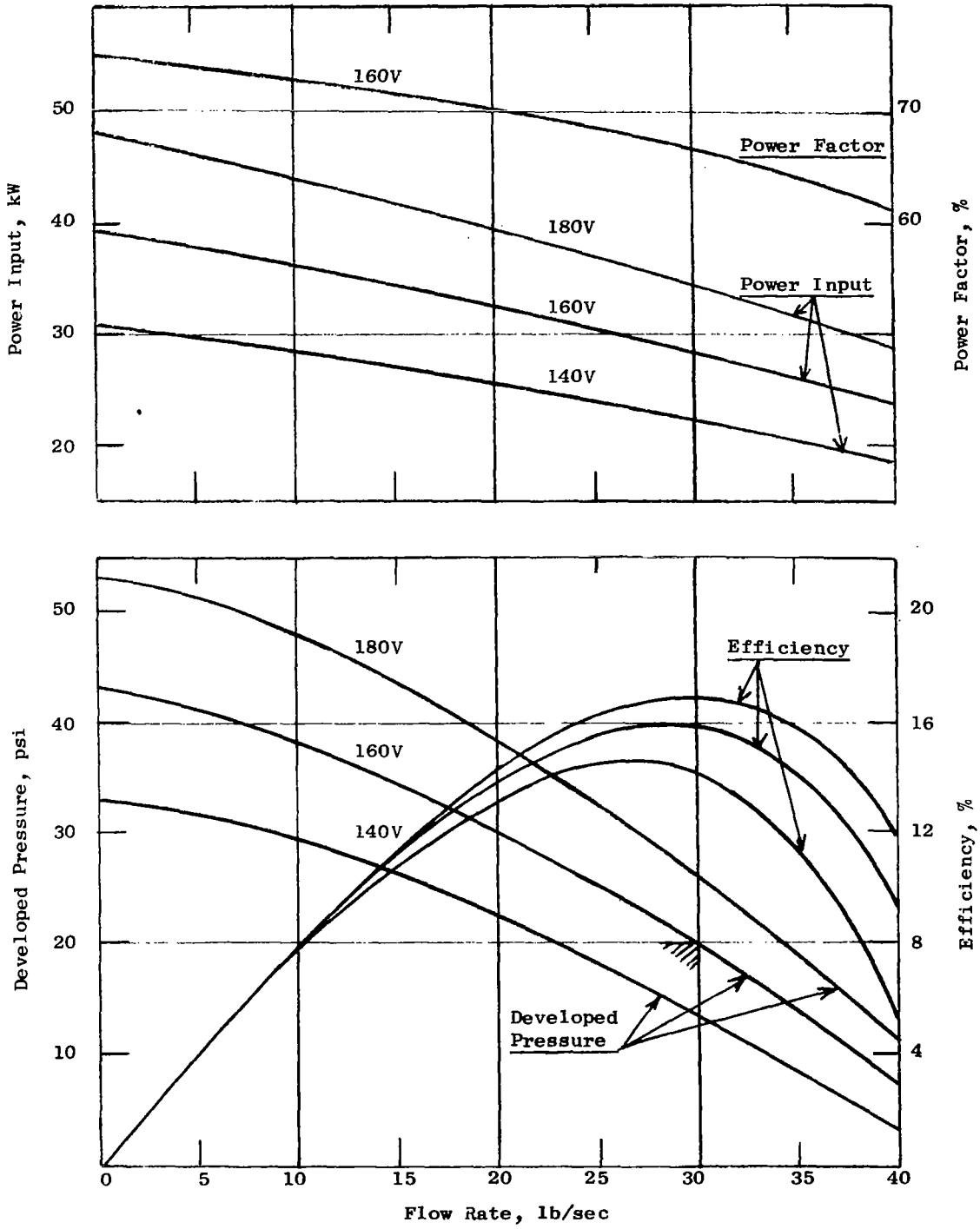

Figure 3. Performance Curves - Helical EM Pump with Center Return (Preliminary Design) with 25 Hz Power Input

NOTE: NaK Coolant Inlet Temperature, 800°F. Design Point Lithium Flow, 30 lb/sec
Lithium Inlet Temperature, 2100°F. Design Point Lithium Δp = 20 psi

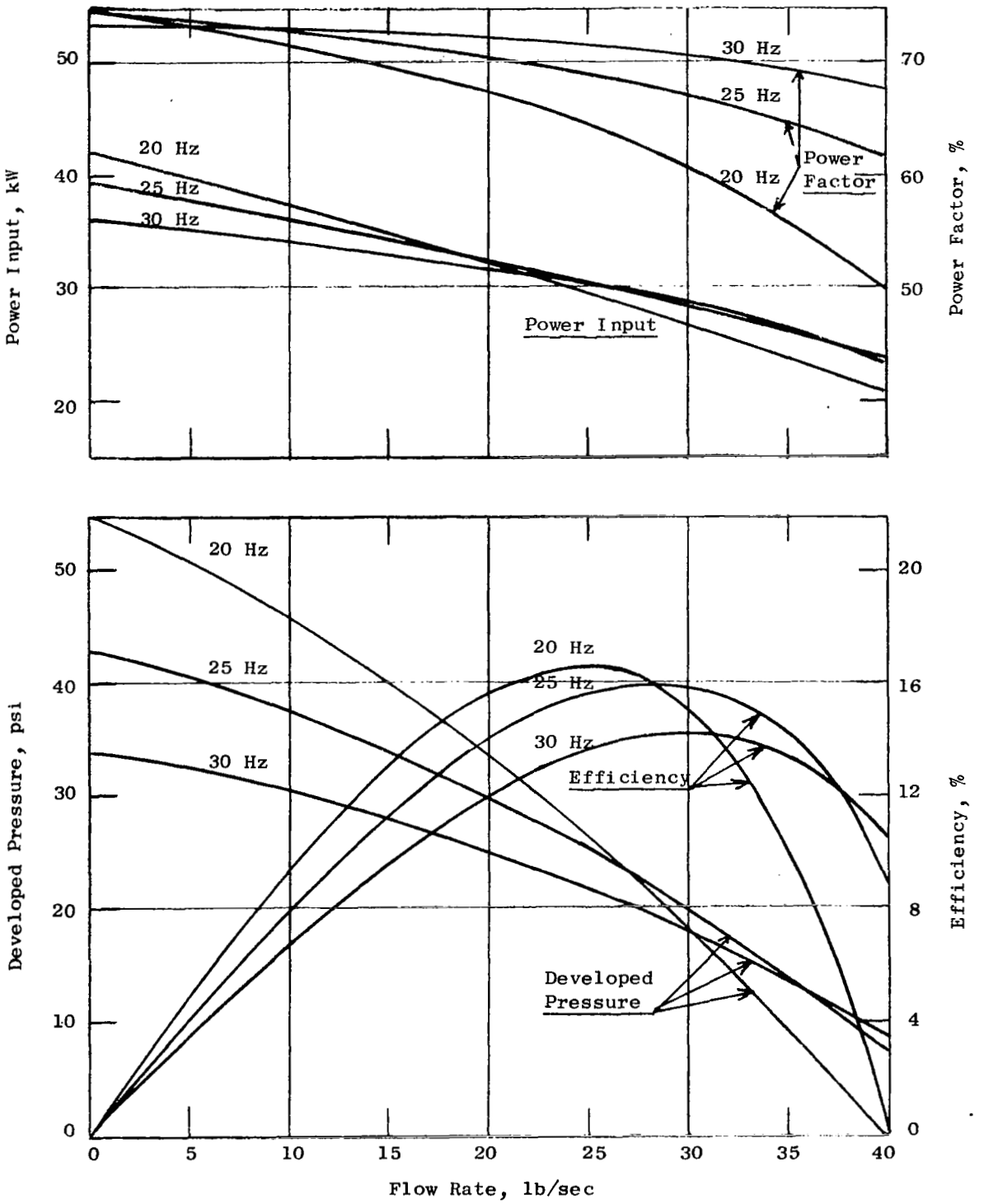

Figure 4. Performance Curves - Helical EM Pump with Center Return (Preliminary Design) with 160V Power Input.

NOTE: NaK Coolant Inlet Temperature, 800°F. Design Point Lithium Flow, 30 lb/sec.
Lithium Inlet Temperature, 2100°F. Design Point Lithium Δp = 20 psi.

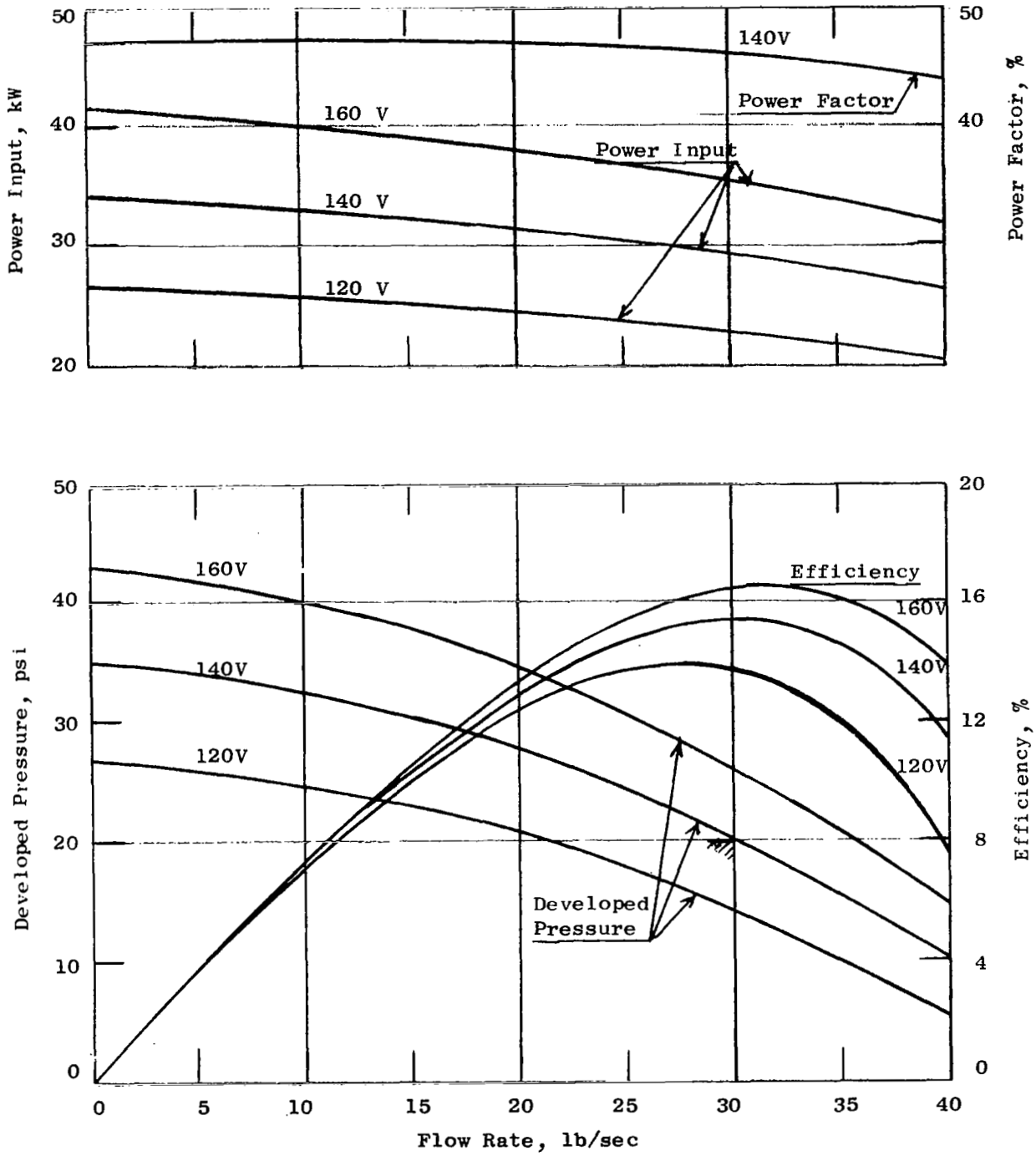

Figure 5. Performance Curves - Helical EM Pump (Preliminary Design) with 60 Hz Power Input.

NOTE: NaK Coolant Inlet Temperature, 800°F. Design Point Lithium Flow, 30 lb/sec.
Lithium Inlet Temperature, 2100°F. Design Point Lithium Δp = 20 psi.

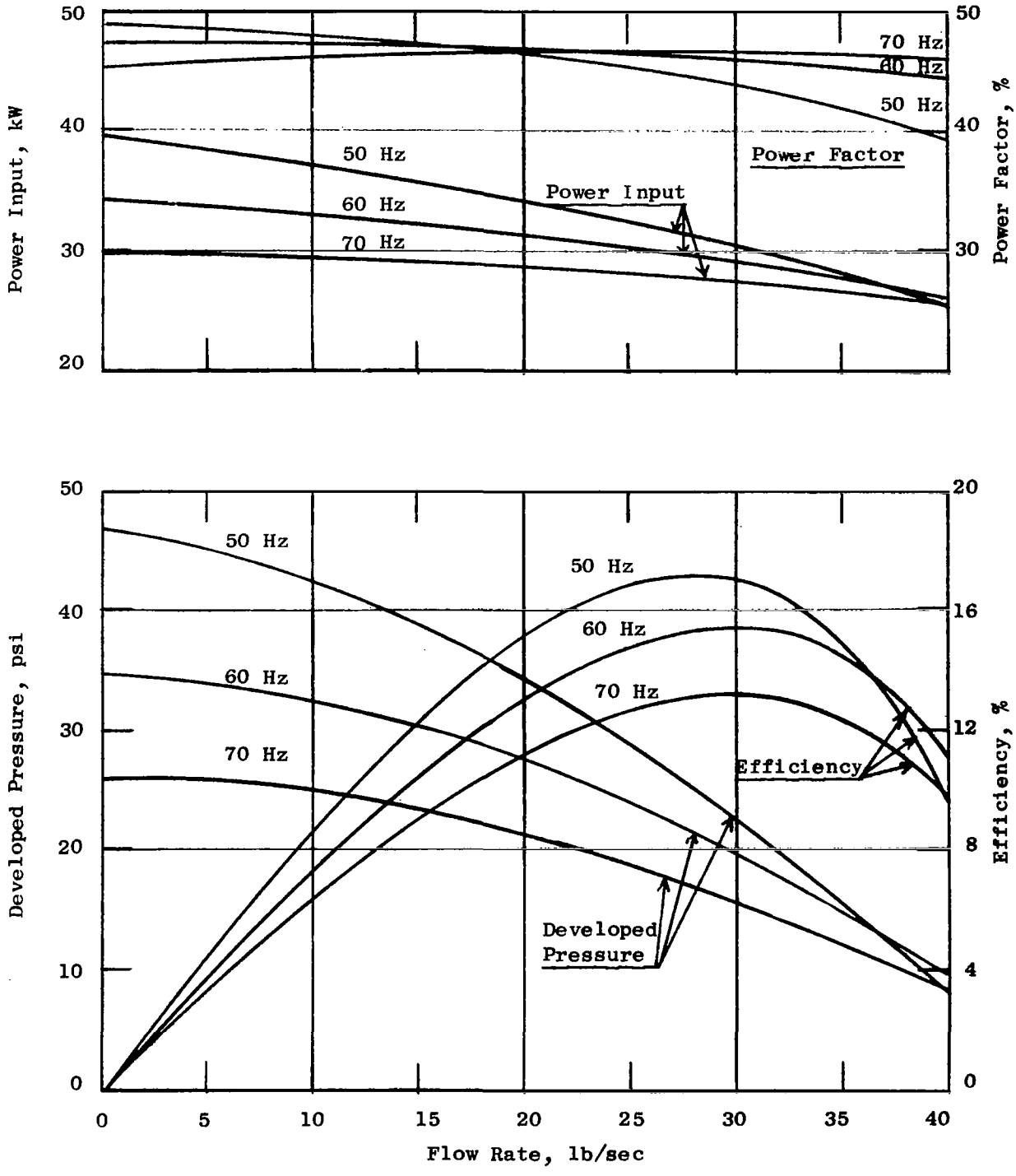

Figure 6. Performance Curves - Helical EM Pump (Preliminary Design) with 140V Power Input.

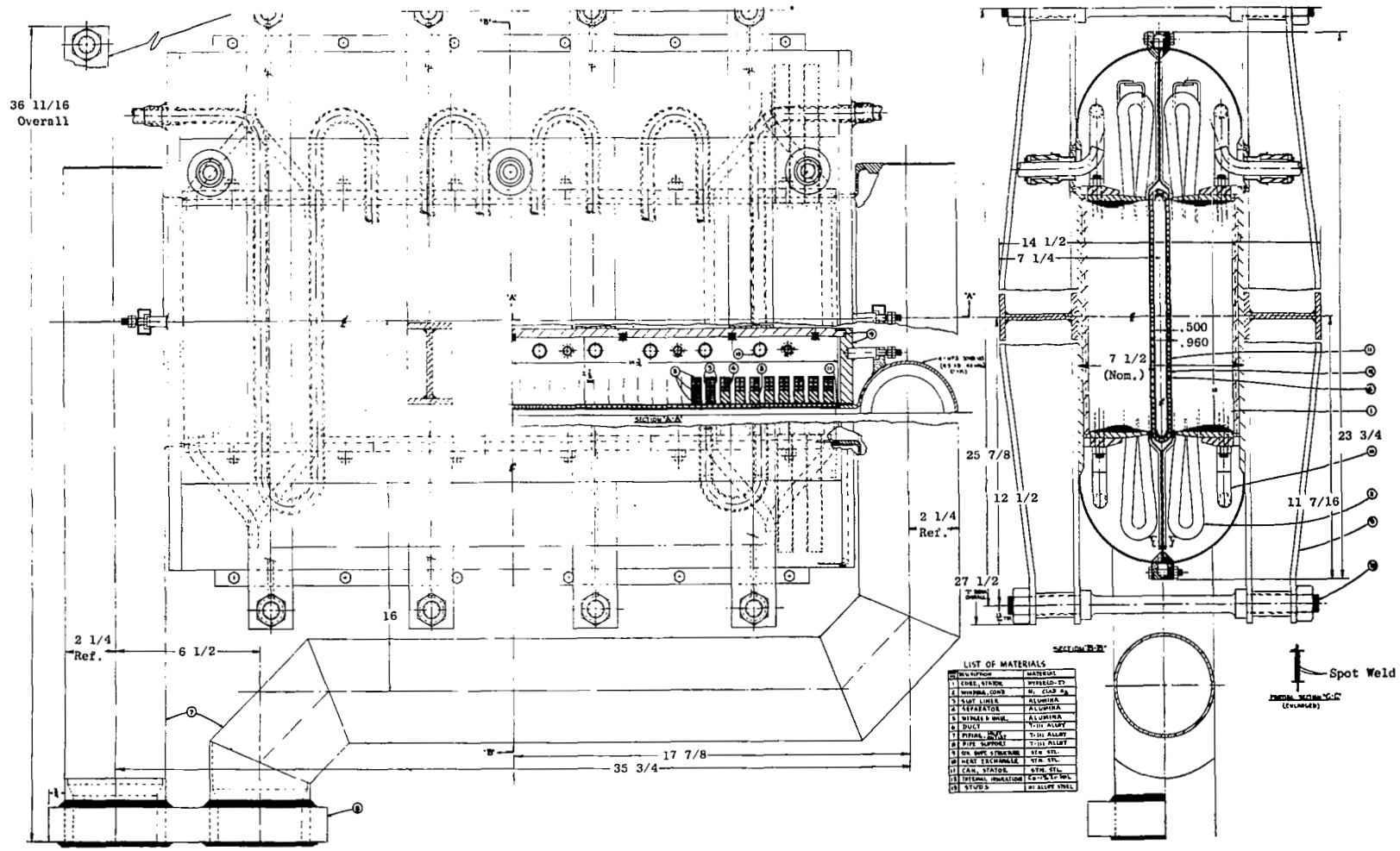

Figure 7. Flat Linear Induction EM Pump. (Preliminary Design)

NOTE: NaK Coolant Inlet Temperature, 800°F. Design Point Lithium Flow, 30 lb/sec.
Lithium Inlet Temperature, 2100°F. Design Point Lithium Δp = 20 psi.

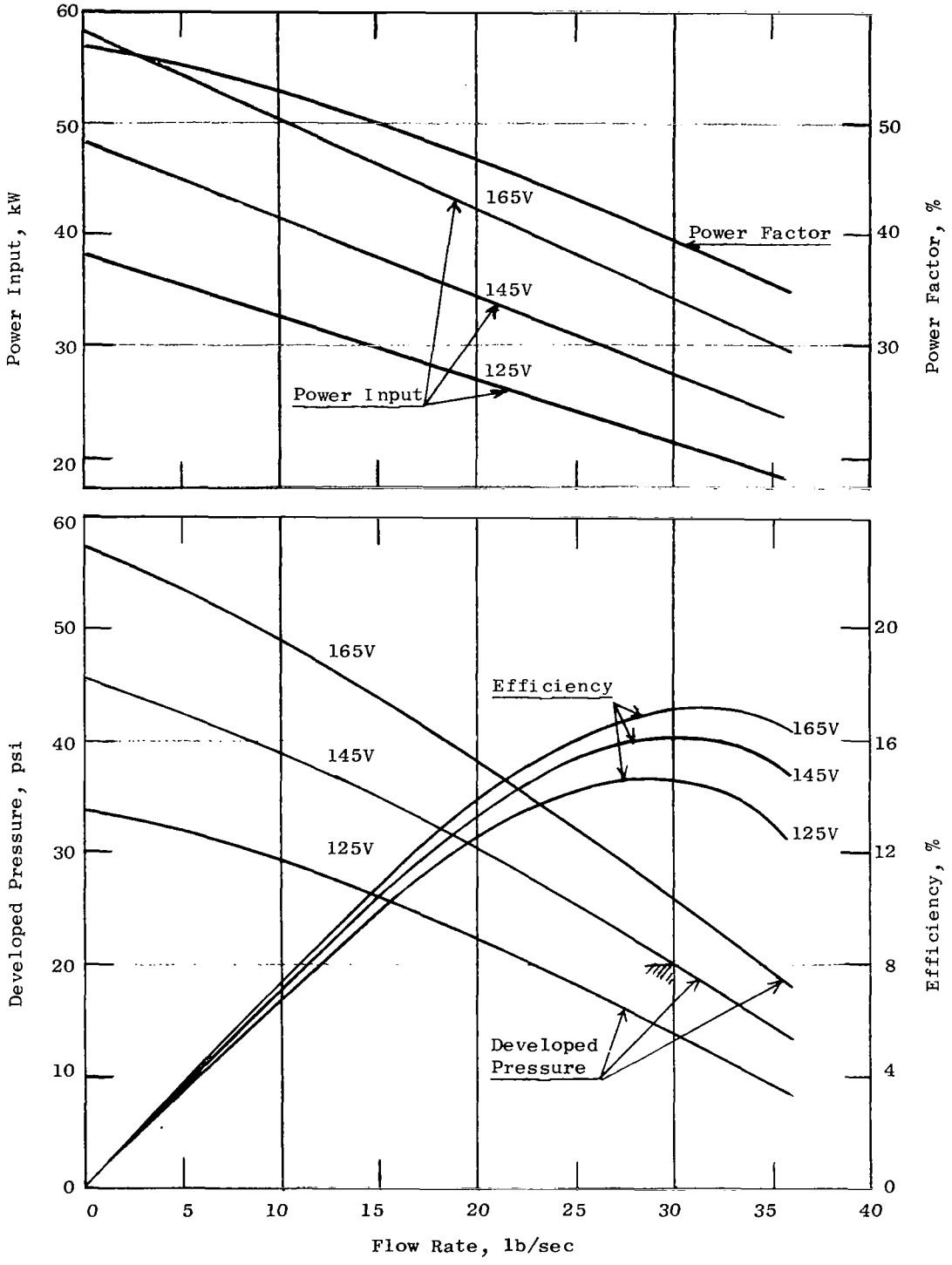

Figure 8. Performance Curves - Flat Linear EM Pump (Preliminary Design) with 60 Hz Power Input.

NOTE: NaK Coolant Inlet Temperature, 800°F. Design Point Lithium Flow, 30 lb/sec.
Lithium Inlet Temperature, 2100°F. Design Point Lithium Δp = 20 psi.

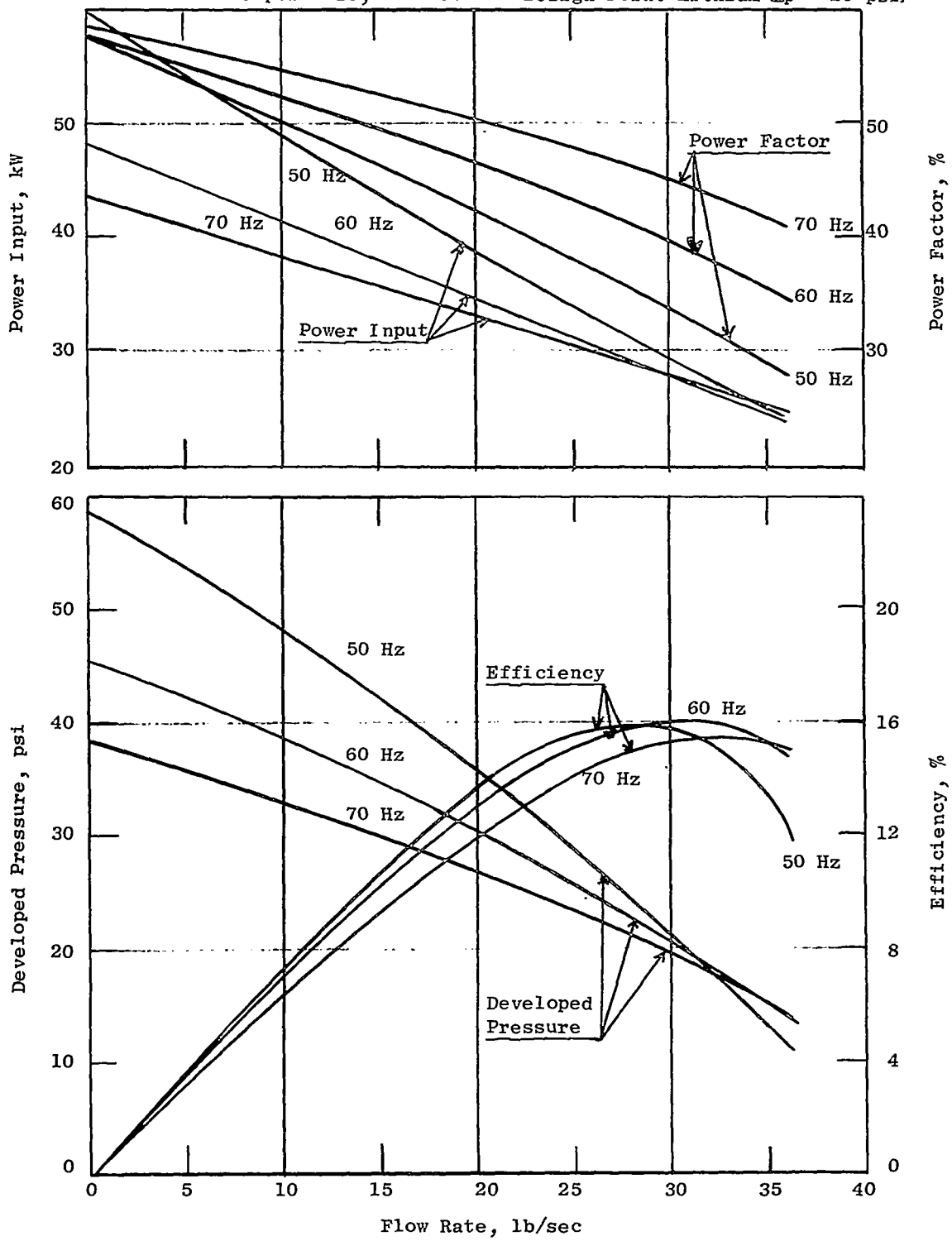

Figure 9. Performance Curves - Flat Linear EM Pump (Preliminary Design) With 145V Power Input.

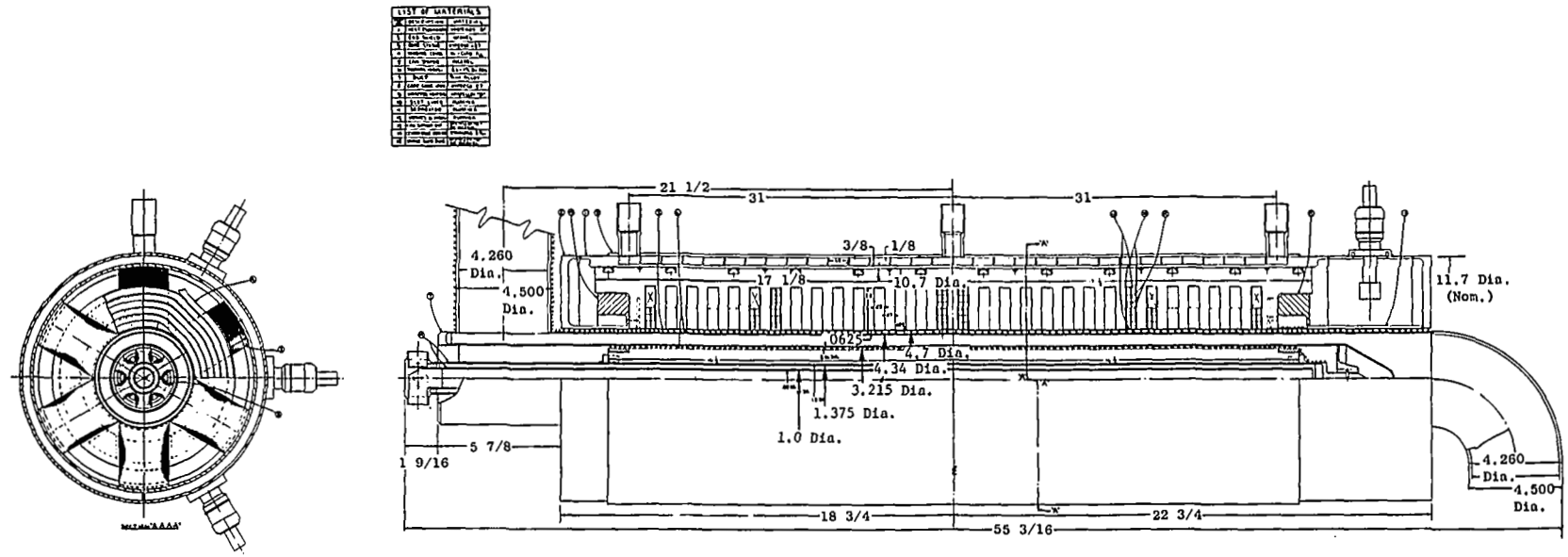

Figure 10. Annular Linear Induction EM Pump. (Preliminary Design)

NOTE: NaK Coolant Inlet Temperature, 800°F. Design Point Lithium Flow, 30 lb/sec.
Lithium Inlet Temperature, 2100°F. Design Point Lithium Δp = 20 psi.

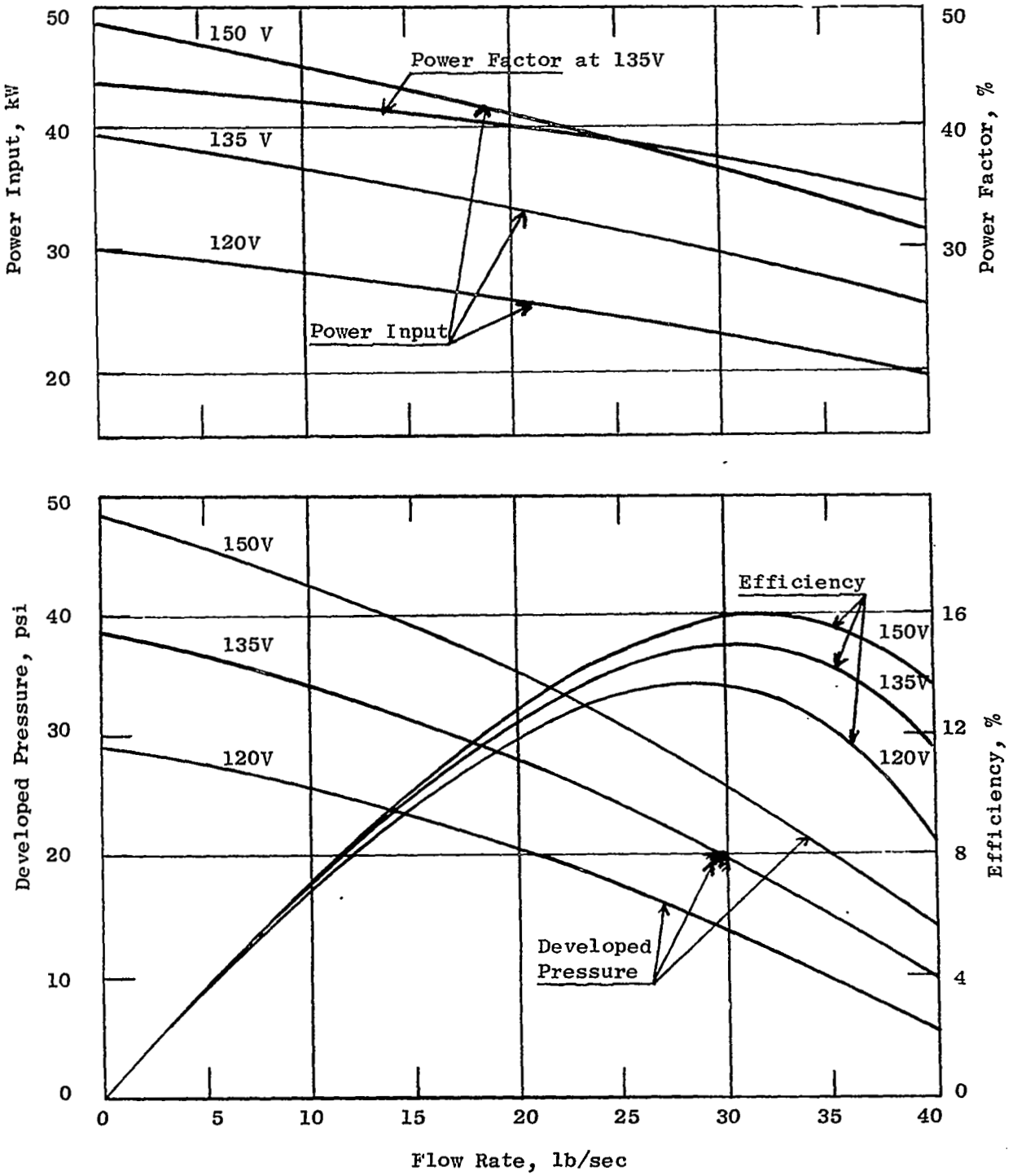

Figure 11. Performance Curves - Annular Linear EM Pump (Preliminary Design) with 60 Hz Power Input.

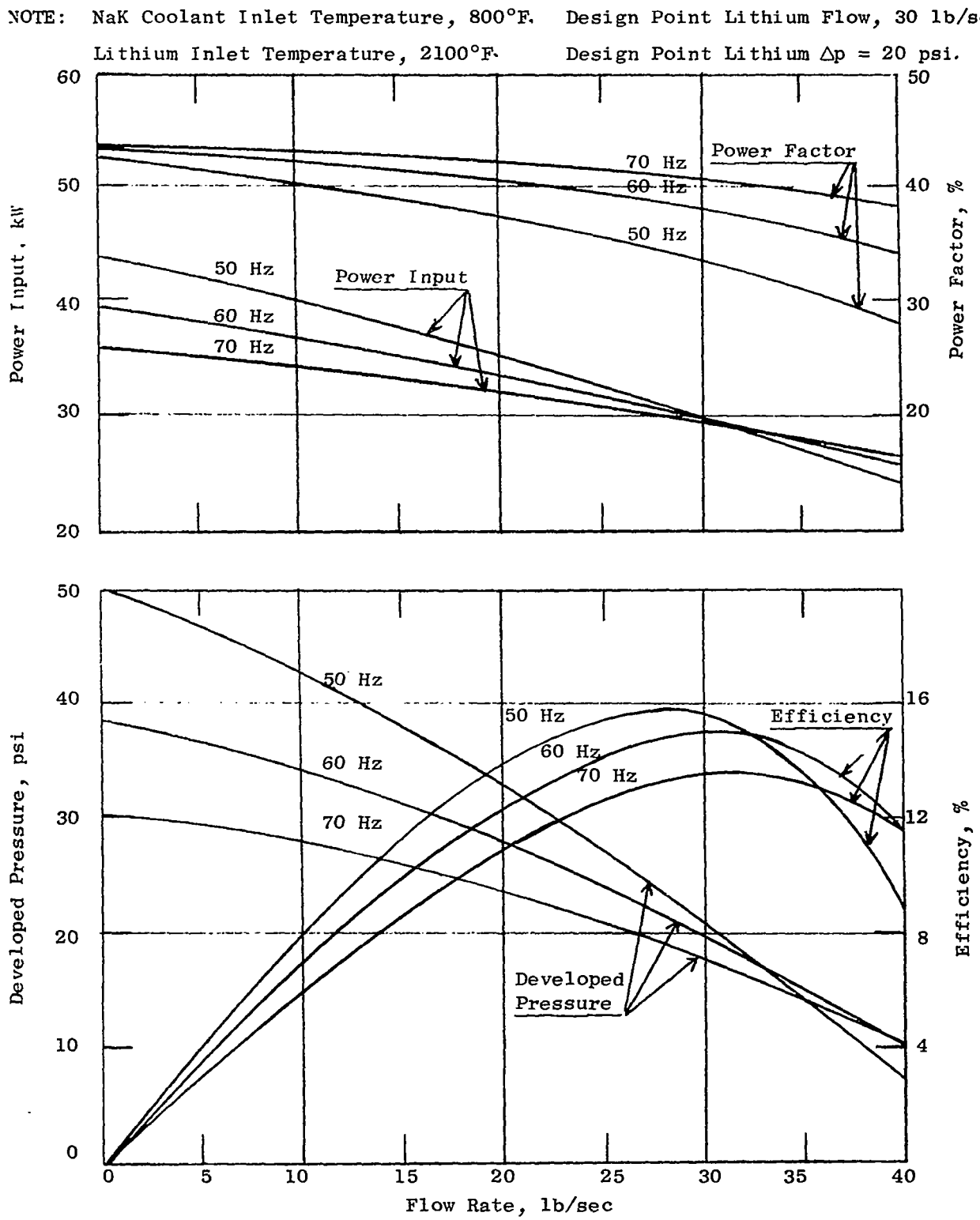

Figure 12. Performance Curves - Annular Linear EM Pump (Preliminary Design) with 135V Power Input.

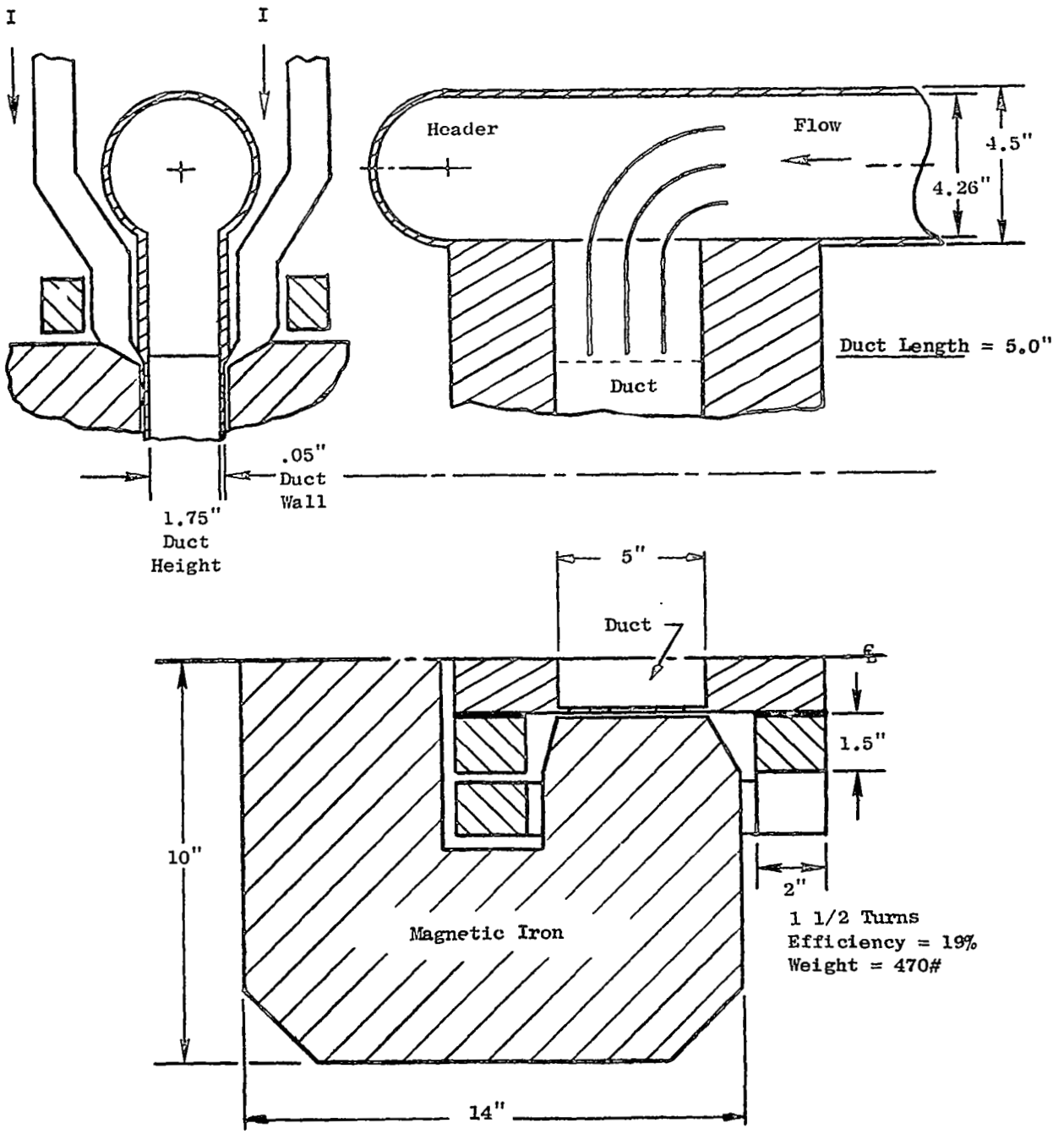

Figure 13. DC EM Pump — Preliminary Design Configuration.

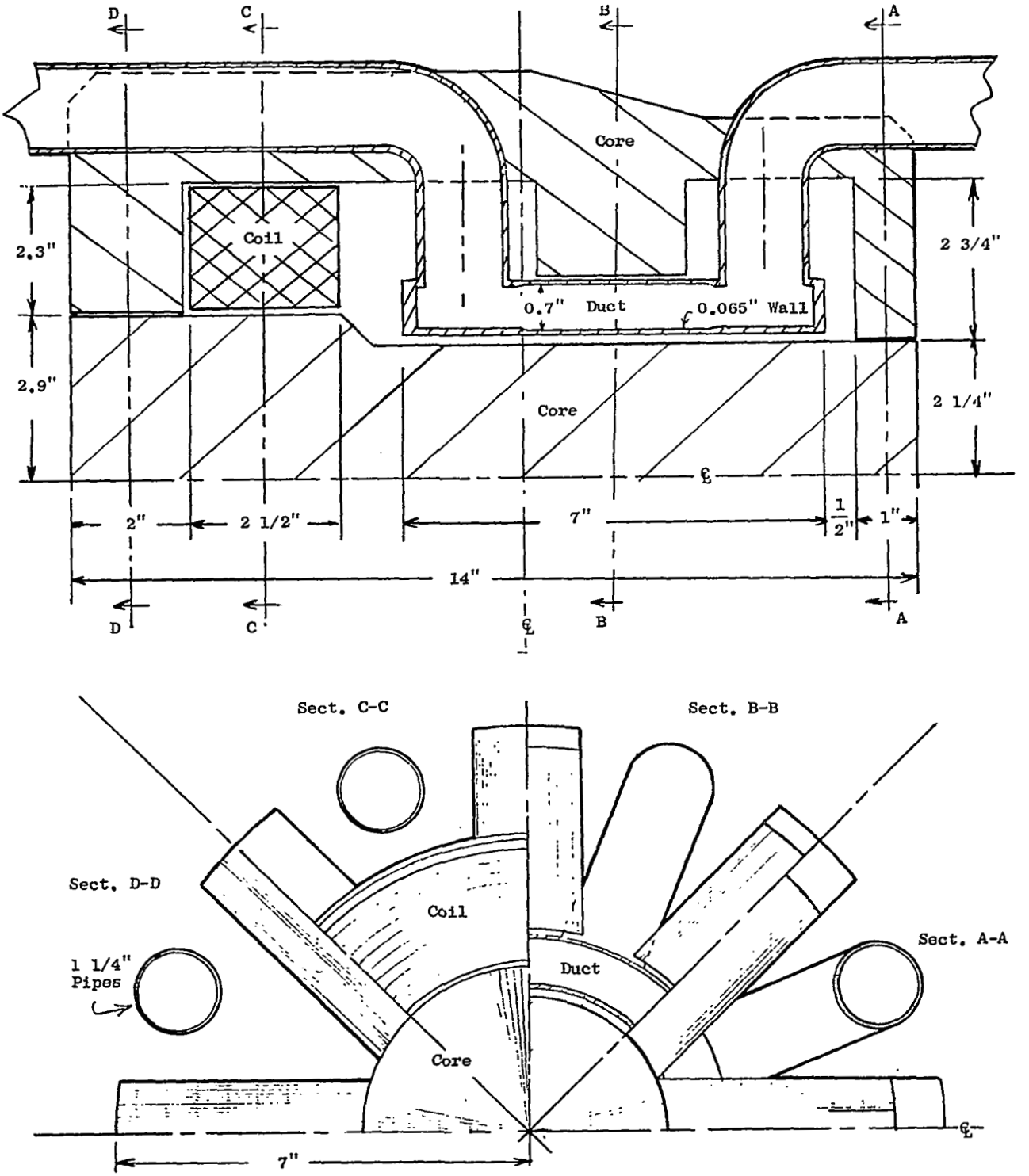

Figure 14. Single Phase EM Pump — Preliminary Design Configuration.

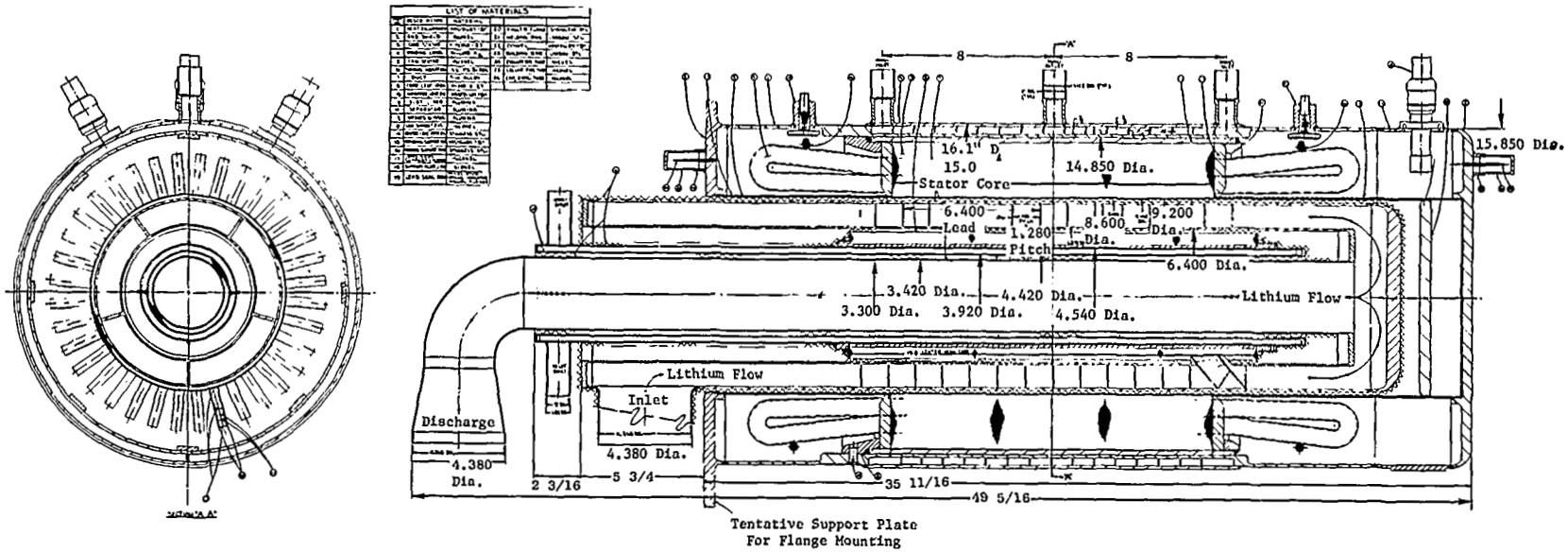

Figure 15. Final Design - Helical Induction EM Pump with Center Return Flow.

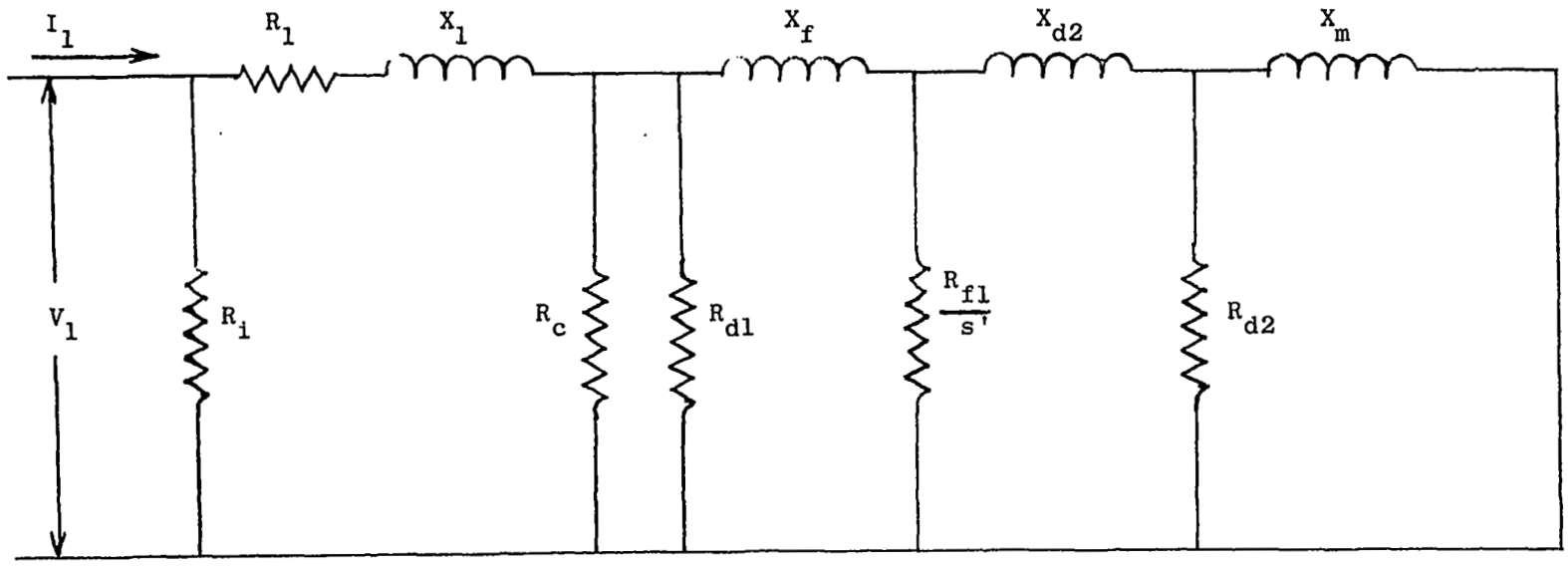

Figure 16. Equivalent Circuit - Helical EM Pump.

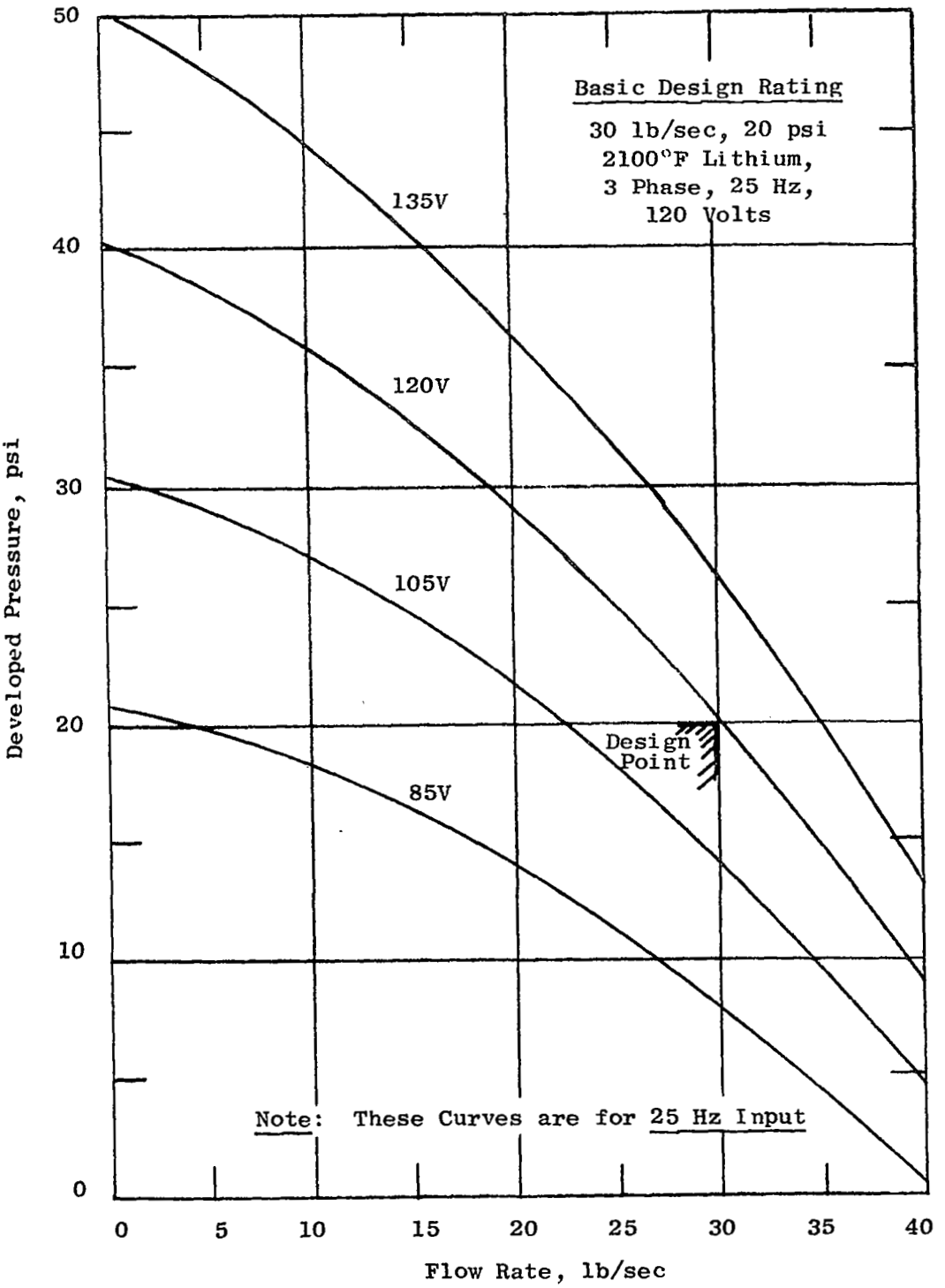

Figure 17. Performance Curves - Helical EM Pump - Final Design.

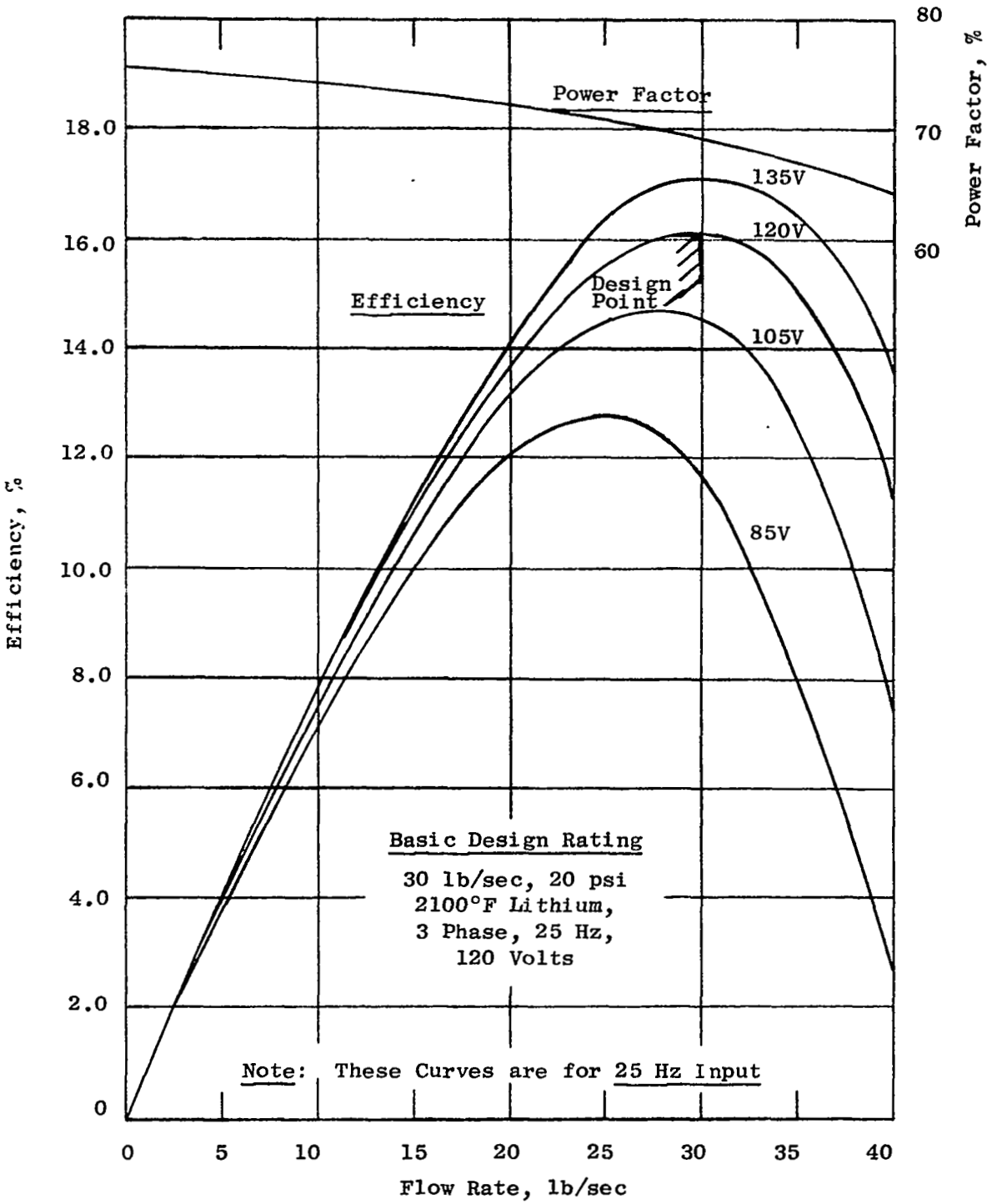

Figure 18. Performance Curves - Helical EM Pump - Final Design

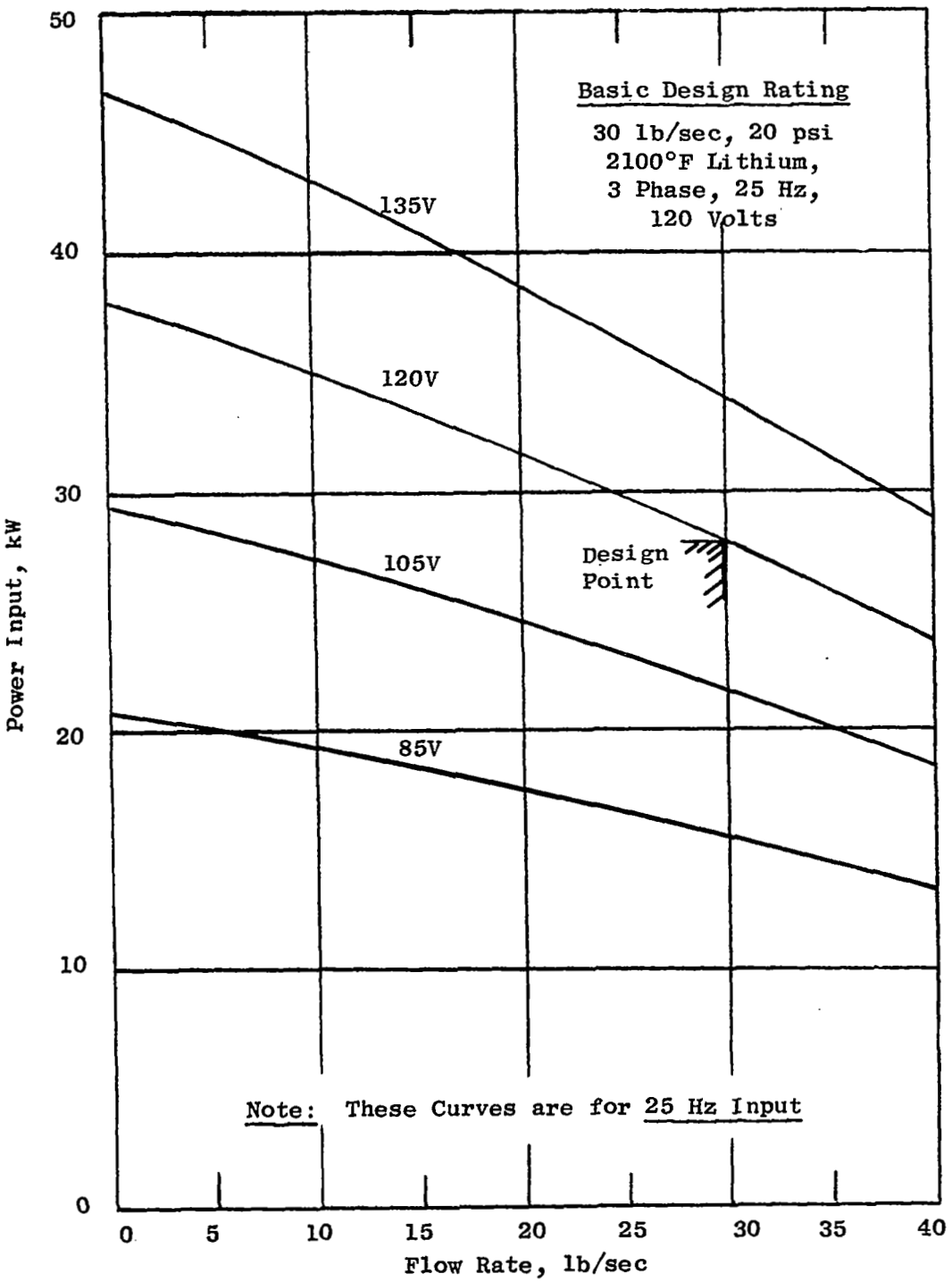

Figure 19. Performance Curves - Helical EM Pump - Final Design.

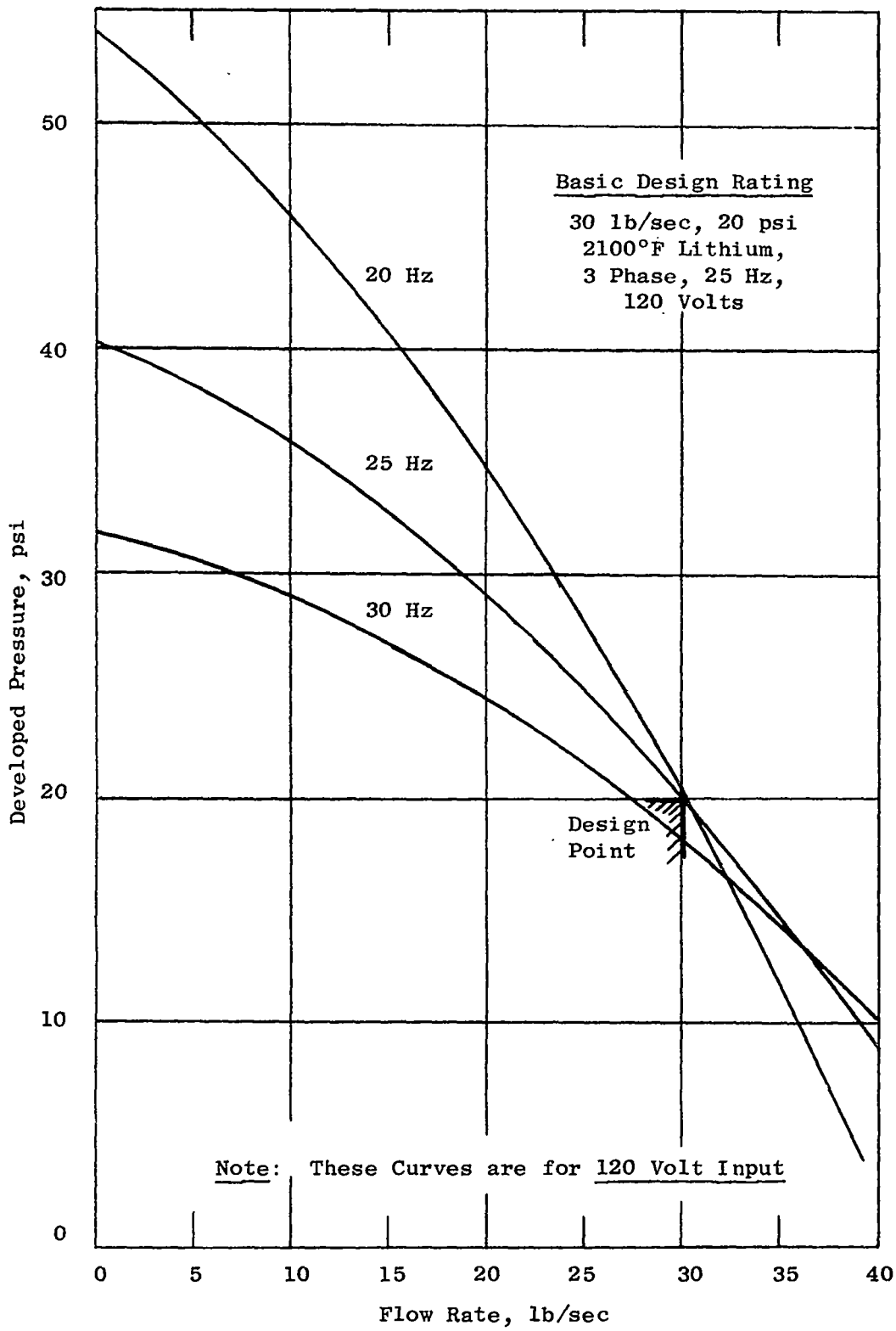

Figure 20. Performance Curves - Helical EM Pump - Final Design.

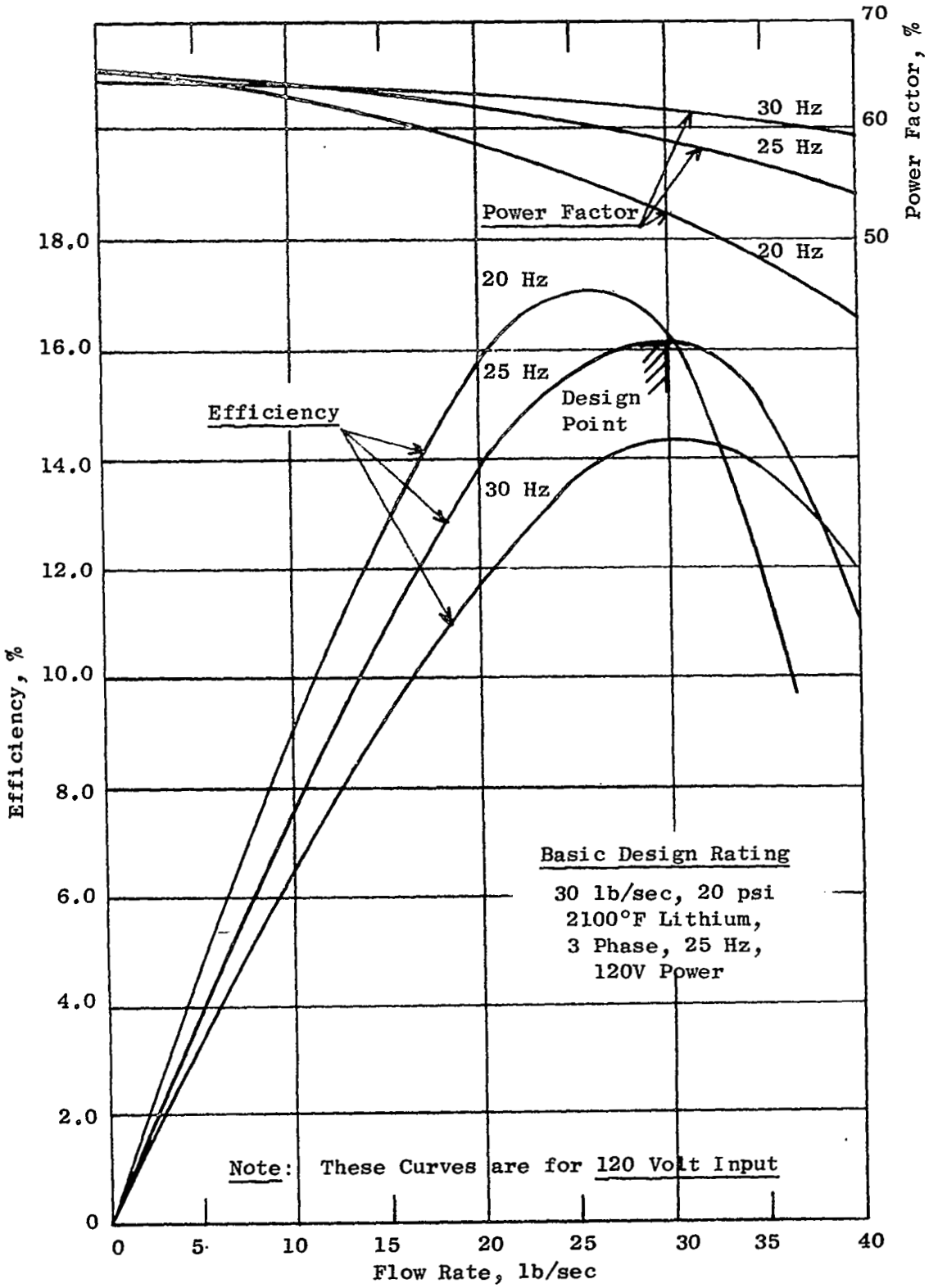

Figure 21. Performance Curves - Helical EM Pump - Final Design.

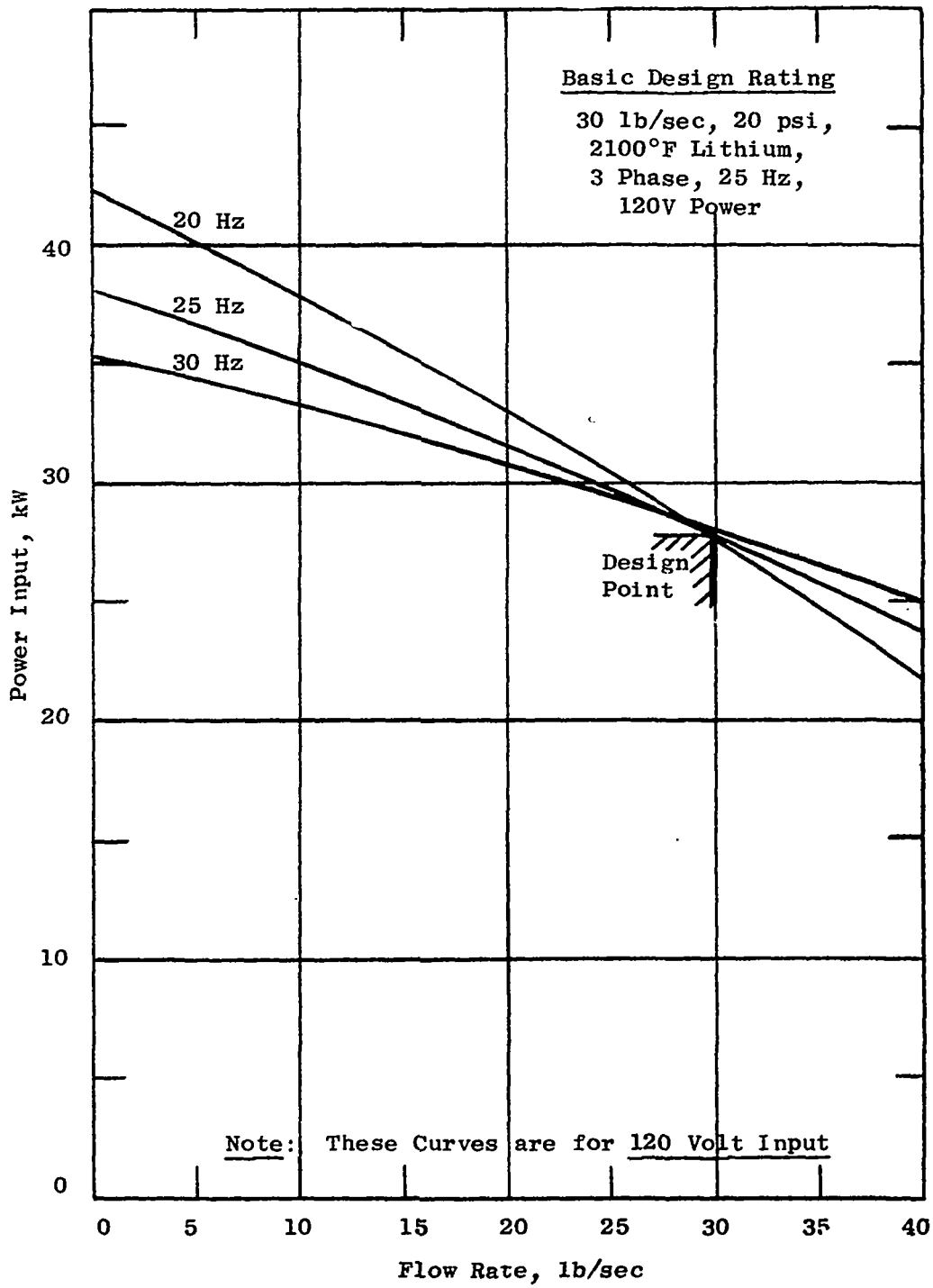

Figure 22. Performance Curves - Helical EM Pump - Final Design.

TABLE 1

CALCULATED DESIGN CHARACTERISTICS

HELICAL INDUCTION EM PUMPS - (Preliminary Designs)

	With Center Return (Fig. 1 - Preferred Design)	No Center Return (Fig. 2)
Frequency	25 Hz	60 Hz
Poles	2	2
Fluid Velocity	25.3 ft/sec	29.7 ft/sec
Slip	0.49	0.58
Duct Wall Thickness	0.1 in.	0.075 in.
Duct Cross Section	8.6 in. OD	5.8 in. OD
Fluid Passage	1.1 in. deep x 6.4 in. lead (4 passages in parallel)	1.4 in. deep x 4.4 in. lead (3 passages in parallel)
Slots/Pole	18	12
Slot Size	0.4 in x 1.9 in approx.	0.5 in x 2.1 in approx.
Stator Size	14.8 in OD x 15 in long x 9 in. bore	12.4 in OD x 18 in long x 6.2 in. bore
Power Input	28.3 kW	29 kW
Efficiency	15.8%	15.4%
Volt Amp Input	42 kVA	63 kVA
Power Factor	67%	46%
Winding Temp. Rise (Above 825°F Coolant)	250°F (Average) 400°F (Hot Spot)	190°F (Average) 310°F (Hot Spot)
Approximate Total Weight	970 lb.	830 lb.
Approximate Overall Dimensions	16.1 in OD x 50 in long	13.7 in OD x 52 in long

TABLE 2

CALCULATED DESIGN CHARACTERISTICS

FLAT LINEAR EM PUMP - (Preliminary Design)

Frequency	60 Hz
Poles	4
Pole Pitch	6 in.
Fluid Velocity	31.5 ft/sec
Slip	0.47
Duct Wall Thickness	0.04 in.
Duct Cross Section	0.58 in. x 11 in.
Fluid Passage	0.5 in. x 10.5 in.
Slots/Pole	9
Slot Size	0.46 in. x 1.15 in. approx.
Stator Size	10 in. stack x 30 in. long
Power Input	27.8 kW
Efficiency	16.2%
Volt-Amp Input	70 kVA
Power Factor	39%
Winding Temperature Rise (Above 825°F Coolant)	180°F (Average) 250°F (Hot Spot)
Approximate Total Weight	960 lb.
Approximate Overall Dimensions	15 in. x 37 in. x 41 in.

TABLE 3

CALCULATED DESIGN CHARACTERISTICS

ANNULAR LINEAR EM PUMP - (Preliminary Design)

Frequency	60 Hz
Poles	4
Pole Pitch	6 in.
Fluid Velocity	28.7 ft/sec
Slip	0.52
Duct Wall Thickness	0.062 in.
Duct Cross Section	4.3 in. OD
Fluid Passage	Annulus 4.18 in OD x 3.18 in ID
Slots/Pole	6
Slot Size	0.55 in. x 2 in. approx.
Stator Size	10.7 in. OD x 30 in. long
Power Input	29.9 kW
Efficiency	15%
Volt-Amp Input	80 kVA
Power Factor	37.6%
Est. Winding Temp. Rise (Above 825°F Coolant)	200°F (Average) 300°F (Hot Spot)
Approximate Total Weight	720 lb.
Overall Dimensions (Approx.)	12 in. OD x 56 in. long

TABLE 4

CALCULATED DESIGN CHARACTERISTICS

DIRECT CURRENT EM PUMP (Preliminary Design)

Series	1.5 (uncompensated)
Fluid Velocity	19 ft/sec
Duct Wall	0.05 in.
Height	1.75 in.
Width	5 in.
Length	5 in.
Magnet Flux Density	15.5 kilogauss
Gap Flux Density	6.75 kilogauss
Current	20,000 A
Volts	1.16 V
Power In	23.2 kW
Efficiency	19%
Approx. Weight	470 lb
Max. Overall Dimension	20 in.

TABLE 5

CALCULATED DESIGN CHARACTERISTICS

SINGLE PHASE INDUCTION EM PUMP (Preliminary Design)

Fluid Velocity	14 ft/sec
Duct Wall	0.065 in.
Duct Diameter	5.25 in.
Height (radial)	0.7 in.
Length	2.5 in.
Frequency	60 Hz
Current*	19,600 A.
Volts*	8.3 V.
Volt-Amp Input	148 kVA
Power Input	69.9 kW
Power Factor	0.43
Efficiency	6.4%
Approx. Weight	435 lb.
Max. Overall Dimension	17 in.

* One turn coil basis; for N turns, multiply coil voltage by N and current by $(\frac{1}{N})$.

TABLE 6

SUMMARY COMPARISON - PRELIMINARY DESIGN

PRINCIPAL CHARACTERISTICS

	Flat	Helical (no center return)	Annular	Helical* (with center return)
Frequency (Hz)	60	60	60	25
Poles	4	2	4	2
Voltage (V)	145	140	135	160
Current (A)	280	260	340	150
Volt-Amp Input (kVA)	70	63	80	42
Power Factor	0.39	0.46	0.376	0.67
Efficiency	0.162	0.154	0.15	0.158
Power Input (kW)	27.8	29	29.9	28.3
KW_{in} x 100 lb/kW	2780	2900	2990	2830
Approximate Weight (lb)	960	830	720	970
Evaluated Weight (lb)	3740	3730	3710	3800
Losses (kW)				
Winding Loss	6.97	6.49	5.8	7.65
Fluid Loss	8.37	11.3	9.86	8.44
Duct & Can Loss	4.97	3.4	6.78	4.5
Average Winding Temp. (°F) (825°F Coolant Ave. Temp.)	1005	1015	1025	1050

*Preferred Design

TABLE 7

SUMMARY COMPARISON - (Preliminary Designs)

PRINCIPAL FEATURES

	Flat	Helical	Annular
Stator			
Punchings	Rectangular Conventional process to make.	Disc Conventional shape.	Rectangular
Unwound core	Two similar sections fabricated independently.	Conventional axial & radial restraint.	To be developed. Several sectors fab. independently. Slot, OD machining. Asm. completed after winding - complex.
Windings	Conventional full coils - Rigid Min. Distortion during insertion. End turn support required.	Conventional Either bar wdgs. with many (≈150) brazed joints, or full coils, severe distortion during insertion. End turn support required - longest end turns.	Unconventional requires development. Leads at OD only. Flexible Turn Insul. Curved Ceramic Pcs. May be rigid, good support once made.
Assembly	Awkward core attachment to frame. Stators assembled independently.	Conventional canned const. Good shrink fit - core to frame.	Core attachment to frame poses problem. Shrink fit weak for heat transfer - Wdgs. must be in place.

TABLE 8

SUMMARY COMPARISON - (Preliminary Designs)

PRINCIPAL FEATURES

	Flat	Helical	Annular
DUCT	Rectangular passage. Flat sheets - not self supporting. Stators provide support. Thermal insulation loaded. difficult design problem at ends. Buckling possible. Friction inhibits some duct motion. No center core required.	Finned cylindrical config. Self-supporting duct. Complex fabrication. Complex flow passage. Simple center magnetic core-washers. Center return flow possible in 25 Hz design with 9 in. bore - permits simpler stator removal and eliminates thermal expansion stresses.	Concentric cylinders. Simple in form. Self supporting. Simplest Fabrication. Awkward center magnetic core-laminations extend axially - difficult to support and assemble.
GENERAL	Least favorable structure and shape. Stators removable w/o cutting duct. Simplest winding.	Experience gained on Boiler Feed Pump. Most established design concept. Most complex duct. Most favorable stator structure. Highest probability of success for these ratings.	No prior experience. Simplest duct.

TABLE 9

ADAPTABILITY OF TYPICAL EM PUMP DESIGNS TO CHANGE IN RATINGS

	Flat	Helical	Annular
Flow Increase to $\geq$ 150%	Good	Poor	Good
Flow Decrease to $\leq$ 50%	Fair	Good	Fair
Pressure Increase to $\geq$ 150%	Poor	Good	Fair
Pressure Decrease to $\leq$ 50%	Good	Fair	Good

TABLE 10

CALCULATED PERFORMANCE CHARACTERISTICS - HELICAL INDUCTION EM PUMP

FINAL DESIGN

Fluid	Lithium
Fluid Temperature (°F)	2100
Flow Rate (lb/sec)	30
Developed Pressure (psi)	20
Power Output (kW)	4.489
Power Input (kW)	28
Efficiency (%)	16
Volt-Amp Input (kVA)	41
Power Factor (%)	68
Weight (lb)	1020
Winding Temperature Rise - Hot Spot (°F)	367
Winding Temperature Rise - Average (°F)	225
Heat Exchanger Requirements*	
- Flow (lb/sec)	2.1
- Pressure Drop (psi)	10
- Total Heat Load (kW)	22.53
- Coolant Inlet Temperature (°F)	800

* Heat exchanger load includes heat transferred from hot lithium which is properly not charged to pump efficiency.

TABLE 11

DETAILED ELECTRICAL DESIGN CHARACTERISTICS

CALCULATED VALUES AT DESIGN POINT (FINAL DESIGN)

Efficiency (%)	16
Power Factor (%)	68
Line Current (A)	200
Line Voltage (V)	120
Losses and Power Requirements	
- Stator Winding I^2R (kW)	7.8
- Iron Loss (kW)	2.0
- Stator Can Loss (kW)	0.5
- Duct Loss (kW)	3.9
- Hydraulic Loss (kW)	1.1
- Fluid (Slip) Loss (kW)	8.2
- Total Losses (kW)*	23.5
- Output (kW)	4.489
- Input (kW)	28
- Input (kVA)	41
Slip	.498
Winding Current Density (A/in^2)	2400
Tooth Peak Flux Density (kilogauss)	3.4
Yoke Peak Flux Density (kilogauss)	9.0
Center Iron Peak Flux Density (kilogauss)	9.1
Gap Peak Flux Density (kilogauss)	2.5

* Charged to Power Input

TABLE 12

HYDRAULIC DESIGN CHARACTERISTICS

Duct Dimensions (Final Design)

Duct Helix	8.6 in. OD
Duct Wall Thickness	0.80 in.
Helix Fluid Passage	1.1 in. deep x 6.4 in. lead
Center Return Tube	3.3 in. ID
Cooling Passage	4.42 in. ID (Outertube) 3.92 in. OD (Innertube)

Calculated Values at Design Point (Final Design)

Velocity of Fluid in Helical Duct (ft/sec)	25.5
Velocity Head of Fluid in Helical Duct (psi)	1.84
Velocity in Center Return Pipe (ft/sec)	19.5
Velocity Head of Fluid in Center Return Pipe (psi)	1.1
Total Hydraulic Loss thru Duct (psi)	4.9

TABLE 13

DETAILED THERMAL DESIGN CHARACTERISTICS

CALCULATED VALUES AT DESIGN POINT (FINAL DESIGN)

Winding Hot Spot Temperature Rise (°F)	367
Winding Average Temperature Rise (°F)	225
Heat Load from Helical Duct through Thermal Insulation (kW) - to Stator	4.3
to Center Core	4
Total Heat Load to Coolant (kW)	23
Heat Load from Center return pipe thru thermal insulation (kW)	4
Heat Load to Stator Heat Exchanger (kW)	14.53
Heat Load to Center Core Heat Exchanger (kW)	8
Total Heat Load to NaK Coolant (kW)	23
Coolant (NaK) Inlet Temperature (°F)	800
Coolant (NaK) Flow Required (lb/sec)	2.1
Coolant (NaK) Pressure Drop (psi)	10
Coolant (NaK) Temperature Rise Through Stator Heat Exchanger (°F)	33
Coolant (NaK) Temperature Rise thru Center Core Heat Exchanger (°F)	17
Coolant (NaK) Total Temperature Rise (°F)	50
Heat Generated in Duct and Fluid (kW)	13.2
Fluid (Lithium) Temperature Rise (°F)	0.5

TABLE 14

DETAILED MECHANICAL DESIGN CHARACTERISTICS (PRESSURE)

CALCULATED VALUES DUE TO PRESSURE LOADING (FINAL DESIGN)

Frame Structure

- Design Pressure	30 psi
- Maximum Primary Hoop Stress in Frame	1 900 psi
- Maximum Stress in End Shield - Conn. End	14 000 psi
- Maximum Stress in End Shield - Opp. Conn. End	13 700 psi
- Maximum Bending Stress in Frame (Primary Pressure + Secondary Bending)	17 700 psi

Duct

- Design Pressure	70 psi
- Maximum Primary Hoop Stress in Duct	2 980 psi
- Maximum Stress in End Cap (Primary Bending)	4 100 psi
- Maximum Bending Stress in Duct (Primary Pressure + Secondary Bending)	7 000 psi

TABLE 15

DETAILED WEIGHT CHARACTERISTICS

CALCULATED VALUES - FINAL DESIGN

Stator	
- Magnetic Core	333 lb
- Winding	226 lb
- Frame and Heat Exchanger	113 lb
- Miscellaneous - End Shields, can support extensions, etc.	130 lb
Duct	
- Helical Duct and Wrapper	110 lb
- Center Magnetic Core and Heat Exchanger	78 lb
- Center Return Flow Parts	30 lb
Total Weight	1 020 lb
Nozzle Connections to Lithium and NaK Loops	10 lb

TABLE 16

POWER SUPPLY REQUIREMENTS

FINAL DESIGN - HELICAL EM PUMP WITH CENTER RETURN

Design Point Flow Rate and Temperature (30 lb/sec at 2100°F)

at 20 psi, developed pressure

Voltage	120 V
Current	200 A
Power Input	28 kW
Volt-Amp Input	41 kVA

at 26 psi, developed pressure

Voltage	135 V
Current	220 A
Power Input	35 kW
Volt-Amp Input	50 kVA

at 14 psi, developed pressure

Voltage	105 V
Current	175 A
Power Input	22 kW
Volt-Amp Input	31 kVA

Off Design Point Flow Rates (extreme points) at 2100°F

35 lb/sec at 10 psi developed pressure

Voltage	105 V
Current	175 A
Power Input	21 kW
Volt-Amp Input	31 kVA

10 lb/sec at 10 psi developed pressure

Voltage	125 V
Current	250 A
Power Input	39 kW
Volt-Amp Input	53 kVA

TABLE 17

EQUIVALENT CIRCUIT PARAMETERS - FINAL DESIGN

(REFER TO FIGURE 16)

R_i	(ohms)	6.9
R_l	(ohms)	0.07
X_l	(ohms)	0.106
R_c	(ohms)	12.1
R_{dl}	(ohms)	2.31
X_{fl}	(ohms)	0.015
R_{fl}	(ohms)	0.19
X_{d2}	(ohms)	0.008
R_{d2}	(ohms)	3.63
X_m	(ohms)	0.316
s'		0.486
s		0.498
I_l	(A)	200
V_l	(V)	69